ISTANBUL TECHNICAL UNIVERSITY ★ GRADUATE SCHOOL OF SCIENCE ENGINEERING AND TECHNOLOGY

A COMPRESSED SENSING BASED APPROACH ON DISCRETE ALGEBRAIC RECONSTRUCTION TECHNIQUE

M.Sc. THESIS

Ezgi DEMİRCAN-TÜREYEN

Department of Computer Engineering

Computer Engineering Programme

JUNE 2015

ISTANBUL TECHNICAL UNIVERSITY ★ GRADUATE SCHOOL OF SCIENCE ENGINEERING AND TECHNOLOGY

A COMPRESSED SENSING BASED APPROACH ON DISCRETE ALGEBRAIC RECONSTRUCTION TECHNIQUE

M.Sc. THESIS

Ezgi DEMİRCAN-TÜREYEN
(504101541)

Department of Computer Engineering

Computer Engineering Programme

Thesis Advisor: Assoc. Prof. Dr. Mustafa Ersel KAMAŞAK

JUNE 2015

İSTANBUL TEKNİK ÜNİVERSİTESİ ★ FEN BİLİMLERİ ENSTİTÜSÜ

AYRIK CEBİRSEL GERİÇATMA TEKNİĞİ İÇİN SIKIŞTIRILMIŞ ALGILAMA ESASLI BİR YAKLAŞIM

YÜKSEK LİSANS TEZİ

Ezgi DEMİRCAN-TÜREYEN
(504101541)

İlgisayar Mühendisliği Anabilim Dalı

Bilgisayar Mühendisliği Programı

Tez Danışmanı: Assoc. Prof. Dr. Mustafa Ersel KAMAŞAK

HAZİRAN 2015

Ezgi DEMİRCAN-TÜREYEN, a M.Sc. student of ITU Graduate School of Science Engineering and Technology 504101541 successfully defended the thesis entitled **"A COMPRESSED SENSING BASED APPROACH ON DISCRETE ALGEBRAIC RECONSTRUCTION TECHNIQUE"**, which she prepared after fulfilling the requirements specified in the associated legislations, before the jury whose signatures are below.

Thesis Advisor :	**Assoc. Prof. Dr. Mustafa Ersel KAMAŞAK** Istanbul Technical University	.....
Jury Members :	**Assoc. Prof. Dr. Mustafa Ersel KAMAŞAK** Istanbul Technical University	.....
	Assoc. Prof. Dr. Ender Mete EKŞİOĞLU Istanbul Technical University	.....
	Asst. Prof. Dr. Ertuğrul SAATÇİ Istanbul Kultur University	.....

Date of Submission : **04 May 2015**
Date of Defense : **02 June 2015**

To Barış,

FOREWORD

First and foremost, I would like to express my gratitude to my advisor Assoc. Prof. Dr. Mustafa E. Kamaşak for his guidance and motivation during my research. I would also like to thank my committee members Asst. Prof. Dr. Ertuğrul Saatçi and Assoc. Prof. Dr. Ender Mete Ekşioğlu for their contributions. Furthermore, the members of Department of Computer Engineering at Istanbul Technical University, as well as at Istanbul Kultur University, are greatly acknowledged. Besides, my sister, Bilge and my parents deserve a deep appreciation for their unconditional support over the years. Finally, I am indebted to my spouse, Barış, for his never-ending patience during my research and I am deeply thankful to him for his selfless support and understanding.

June 2015

Ezgi DEMİRCAN-TÜREYEN
Computer Engineer

TABLE OF CONTENTS

Page

ABBREVIATIONS

ARM	**:** Algebraic Reconstruction Method
ART	**:** Algebraic Reconstruction Technique
CS	**:** Compressed Sensing
CT	**:** Computed Tomography
DART	**:** Discrete Algebraic Reconstruction Technique
DT	**:** Discrete Tomography
FBP	**:** Filtered Backprojection
IRT	**:** Iterative Reconstruction Techniques
MAP	**:** Maximum a posteriori Probability
MRI	**:** Magnetic Resonance Imaging
NP-hard	**:** Non-deterministic Polynomial-time hard
PDM	**:** Projection Distance Minimization
RMSE	**:** Root Mean Squared Error
RMSPE	**:** Root Mean Squared Projection Error
SART	**:** Simultaneous Algebraic Reconstruction Technique
SIRT	**:** Simultaneous Iterative Reconstruction Technique
SPECT	**:** Single-photon Emission Computed Tomography
TSMO	**:** Two-stage Multi-level Otsu Thresholding
TV	**:** Total Variation
TVAL3	**:** TV minimization scheme based on Augmented Lagrangian and Alternating Direction Algorithms
TvMin	**:** Total Variation Minimization
VE	**:** Valley Estimation

LIST OF FIGURES

Page

A COMPRESSED SENSING BASED APPROACH ON DISCRETE ALGEBRAIC RECONSTRUCTION TECHNIQUE

SUMMARY

Image reconstruction from incomplete projections has a crucial meaning in tomographic imaging field, due to some restrictions and requirements. Although the analytical methods, such as filtered backprojections (FBP), are preferable because of their low computational cost; they are not good at reconstructing satisfying images in case of limited number of projections and limited view. On the other hand, iterative methods (e.g. algebraic reconstruction technique (ART), norm optimization) makes the reconstruction from incomplete projection data possible. The ART (as well as its variations) models the reconstruction problem as a system of linear equations where the discretization points (i.e. pixels) of the image are variables and the equations represent the projections. For these algebraic reconstruction methods (abbreviated ARM), there is no unique solution due to the under-determined characteristic of the system, when the incomplete projection data is the case. Many iterative methods take some constraints into consideration and some of those methods suggest to exploit prior knowledge, if exists, in order to find the best approximation to the exact solution. The field of discrete tomography (DT) assumes that the variables have a range (and sometimes domain) of a finite and discrete set, whose element count is few and known a priori; and it aims to find a good quality solution even if the projection samples are highly reduced. Compressed sensing (CS) based methods, in the other respect, aims to find the sparsest solution by assuming the image is sparse in a known domain. Both approaches are used to be able to recover images from the projection data which doesn't satisfy the Nyquist-Shannon criterion.

Discrete algebraic reconstruction technique (DART), which is a technique used in DT field and lies at the core of this study, accomplishes the goal stated above by combining a continuous ARM and a discretization scheme, in an iterative manner. In this study, the DART algorithm is investigated and it is combined with an initial total variation minimization (TvMin) technique, which is used to solve CS problems, to ensure a better initial guess. Also, the algorithm is extended with a segmentation procedure in which the threshold value, which simultaneously minimize both the projection error and the total variation (TV), is selected from a finite set of candidates, obtained using a histogram based thresholding scheme. Furthermore, the algorithm is extended with a gray level estimation procedure, which serves as an automatic determination of the gray levels to be used in the discretization step. A formulation is presented in order to approximate the exact gray levels and it is shown that the gray levels can almost be computed, even though they are not known in advance. All implementations are done using MATLAB environment. The proposed algorithm is compared to the DART and the FBP algorithms by the simulation experiments which are done under the conditions of limited number of projections, limited view and noisy projections, and the computational results are presented visually, either via the reconstructed images or the graphics.

AYRIK CEBİRSEL GERİÇATMA TEKNİĞİ İÇİN SIKIŞTIRILMIŞ ALGILAMA ESASLI BİR YAKLAŞIM

ÖZET

Bilgisayarlı tomografide, x-ışınları ile taranan nesnenin iki boyutlu kesit görüntüsünün bir boyutlu izdüşüm veri kümesinden geri çatımı problemi, analitik yöntemlerle veya yinelemeli olarak çözülebilmektedir. Geleneksel filtreli ters izdüşüm tekniği (FBP) başta olmak üzere, bu amaçla kullanılan analitik yöntemler, merkezi kesit teoremine dayanmaktadır. Bu yöntemler hesaplama karmaşıklığının düşük olmasından dolayı tercih edilir olsalar da, Nyquist-Shannon kıstasını karşılayamayacak kadar sınırlı sayıda veya sınırlı açısal aralık ile toplanan izdüşümlerden kaliteli görüntüler elde etme konusunda başarısızdırlar. Ancak tomografik görüntülemede, bir görüntünün eksik izdüşüm verisinden eksiksize yakın bir şekilde geri çatımı, çeşitli kısıt ve gereksinimlerden dolayı kritik öneme sahiptir. Bu nedenle, cebirsel geriçatma ve norm optimizasyonu gibi yinelemeli yöntemler, çeşitli varsayımlar kullanıldığı takdirde eksik veri ile geri çatımı olanaklı kıldığı için, tercih edilmektedir.

Cebirsel yöntemler, geriçatma problemini, değişkenlerin görüntünün ayrık bileşenleri (çoğunlukla pikseller) olduğu ve elde edilen izdüşümlerin denklemler ile ifade edildiği bir lineer denklem sistemi olarak formüle eder ve bu sistemin çözümüne yinelemeli olarak yakınsamaya çalışır. Bu sistemde her bir denklem bir izdüşüm ölçümünün, ilgili ışının taradığı piksellerin ağırlıklı toplamı olduğunu (buna doğru integrali de denmektedir) ifade eder. Bahsedilen lineer denklem sistemi için izdüşüm verisinin eksik olması durumunda, sistem kararsız özelliktedir ve tek bir çözümden bahsedilemez. Bu önerme uygulamada, bir izdüşüm veri kümesinin birden fazla imgeye ait olabileceği gerçeğine karşılık düşer. Bu tip kararsız sistemler için çözüm getiren Kaczmarz metodu, her iterasyonda mevcut kestirimi hiperdüzlemlere iz düşürerek güncellemeyi önermektedir. Cebirsel geriçatma tekniği (ART), eşzamanlı yinelemeli geriçatma tekniği (SIRT) ve eşzamanlı cebirsel geriçatma tekniği (SART) gibi cebirsel geriçatma algoritmaları, Kaczmarz metoduna dayanmaktadır. Toplanan izdüşüm verisi miktarı oldukça kısıtlı olduğunda bile kaliteli görüntüler elde edebilmek için, yinelemeli teknikler, önsel bilgi ve varsayımlardan faydalanarak yeniden geliştirilmektedir. Buna, bu çalışmanın da temelini oluşturan, ayrık tomografi (DT) alanı ve sıkıştırılmış algılama (CS) teoremine dayanan yöntemler örnek olarak gösterilebilir. Ayrık tomografi, görüntü bileşenlerinin sonlu ve ayrık bir değer kümesinden (ve hatta kimi durumlarda tanım kümesinden) geldiği varsayımı ile, ve taranan nesnenin az sayıda farklı yoğunluk derecelerinden oluştuğu önşartını koyarak, gereken izdüşüm verisini bir hayli azaltmayı amaçlamaktadır. Diğer taraftan, sıkıştırılmış algılama (CS) teoremini temel alan yöntemler ise, bir görüntünün kendisinin veya bilinen bir dönüşüm alanındaki temsilinin seyrek olduğu varsayımı ile, en seyrek çözümü bulmayı hedeflemektedir.

Yukarıda bahsedilen amaçlarla geliştirilmiş ve ayrık tomografi alanında kullanılmakta olan ayrık cebirsel geriçatma tekniği (DART), birbirini izleyen; cebirsel geriçatma,

geriçatma görüntüsünü ayrıklaştırma ve değişken azaltma aşamalarından oluşan bir algoritmaya sahiptir. Bu algoritmada her bir iterasyon için, ART, SART veya SIRT kullanılarak bir geriçatma görüntüsü hesaplanır ve sonrasında bu görüntü üzerinde, Otsu eşikleme algoritmasına göre histogram üzerinden elde edilen eşik değerler ve gerçek görüntüdeki gri seviyelere dair önsel bilgi parametreleri ile segmentasyon uygulanır. Burada, eşik değer belirleme amaçlı kullanılan Otsu yöntemi yerine, mevcut izdüşüm verisinden faydalanarak izdüşüm hatasını enküçültecek eşik değerlerini seçmeye yönelik bir yaklaşım da önerilmiştir. DART algoritması aynı zamanda her iterasyonda, sistemi daha az kararsız hale getirmek adına, segmentasyon sonrası yanlış değerlere atanmış olma ihtimali daha yüksek olan sınır bölgelerin dışındaki tüm pikselleri sabitler ve geriçatma işlemine sabitlenmeyen pikseller ile devam eder.

Sıkıştırılmış algılama teoremini temel alan yöntemler ise seyrek olduğu bilinen sinyaller için, en seyrek çözümü bulmak adına sinyalin ℓ_1 normunu ($\ell_0 -$ *minimizasyonu* ve $\ell_1 -$ *minimizasyonu* özdeşliğine dayanarak) enküçültmeye çalışır. Çoğu bilgisayarlı tomografi görüntüsünde olduğu gibi sinyalin kendisinin seyrek olmaması durumunda ise, sinyali seyrekleştiren dönüşümlerden faydalanılır ve bu sefer, sinyalin dönüştürüldüğü uzaydaki temsili için $\ell_1 -$ *minimizasyonu* uygulanır. Sinyalin seyrek temsilini frekans uzayında aramak için kullanılan dalgacık (Wavelet), Fourier gibi dönüşümler dışında, seyrekleştirmeyi imge uzayında gerçekleştiren dönüşümler de kullanılmaktadır. Toplam değişintinin minimizasyonu tekniği (TvMin), ikinci tipte bir dönüşüm olan ayrık gradyan dönüşümünden faydalanır. Ayrık gradyanın ℓ_1 normuna toplam değişinti (TV) denilmektedir ve amaç, bu toplam değişinti miktarını, izdüşüm hatasını da sıfıra yakın bir eşiğin altında tutacak şekilde enküçültmektir. En bilinen hali ile toplam değişinti minimizasyonu problemi, izdüşüm hatasını kısıt olarak kullanmak yerine, toplam değişinti terimi ile birlikte amaç fonksiyonuna dahil ederek formüle edilmektedir. TvMin tekniği, görüntünün yüksek frekanslı bileşenlerini koruyabilme özelliğinden dolayı, görüntü geriçatma ve gürültü giderme amacıyla, sıklıkla tercih edilmektedir.

Bu çalışmada DART algoritmasını TvMin tekniğinden de faydalanarak geliştirmek amaçlanmış ve bu doğrultuda DART üzerinde bazı değişiklikler öneren bir algoritma sunulmuştur. Öncelikle, daha iyi bir ilk kestirim elde edebilmek amacıyla, DART'ta kullanılan cebirsel geriçatma yönteminin, sadece ilk kullanım için TvMin ile değiştirilmesi önerilmiştir. Bu sayede, tez kapsamında sunulmuş olan deney sonuçlarından da görülebileceği üzere, segmentasyona daha uygun bir görüntü elde edilebilmektedir. Ayrıca, önerilen algoritma, DART algoritmasının sürekli görüntüyü ayrıklaştırma amacıyla kullandığı segmentasyon yöntemi üzerinde durmakta ve bunun yerine kullanılabilecek iki aşamalı bir eşik değeri seçme prosedürü ileri sürmektedir. Histograma ve izdüşüm hatasına dayalı iki yaklaşımı birleştiren bu prosedürün ilk aşamasında, iki kademeli çok düzeyli Otsu (TSMO) algoritması kullanılarak, histogramdaki vadi sayısı kadar aday eşikleme değeri hesaplanmakta; ikinci aşamasında ise bu adaylar arasından, izdüşüm hatası ile birlikte toplam değişintiyi enküçülten eşik değeri seçilmektedir. Böylece hem geri çatılan görüntü hem de izdüşüm ölçümleri ile tutarlı eşik değerleri seçilebilmekte, gerçek görüntüye daha yakın sonuçlar hesaplanabilmektedir. Çalışma kapsamında ele alınan son nokta ise, ayrıklaştırmada kullanılacak olan gri seviyelerin önceden bilinmemesi veya yanlış bilinmesi halinde, algoritma tarafından tahmin edilebilmesi hususudur. Bu amaçla kullanılabilecek bir formülasyon sunulmuş ve gri seviyelerin, gerçek değerlerine oldukça yakın bir şekilde hesaplanabildiği, ilgili deney sonuçları ile gösterilmiştir.

Deneylerde her biri iki gri seviyeden oluşan, beş farklı sentetik görüntü (fantom) kullanılmıştır. Önerilen algoritma, her bir fantom için, DART ve FBP algoritmaları ile sınırlı sayıda izdüşüm, sınırlı açısal aralık ve gürültülü veri gibi koşullar simüle edilerek karşılaştırılmıştır. Ek olarak, bu üç algoritmanın uzaysal çözünürlüğü, farklı frekanslara karşılık düşen test örüntüleri kullanılarak sınanmıştır. Uygulamaların tamamı MATLAB ortamında gerçeklenmiş olup, deneyleri sonuçları, grafikler ve elde edilen geriçatma görüntüleri kullanılarak sunulmuştur.

1. INTRODUCTION

The following document is organized into six chapters. Chapter 1 serves as an introduction to the succeeding chapters. It presents a background first, next exemplifies some studies from the literature and finally introduces the hypothesis. Chapter 2 describes the principles of the tomographic reconstruction problem and merely examines the analytic and algebraic reconstruction methods. Chapter 3 narrows the reconstruction problem, introduced in the previous chapter, down to a reconstruction from small number of projections problem and presents discrete tomography and compressed sensing concepts. In Chapter 4, the proposed method is yet described, by first introducing the DART algorithm and TvMin technique, respectively. In Chapter 5, the simulation experiment results are presented by considering several conditions and comparing the proposed method with the DART algorithm and finally, Chapter 6 is reserved for the conclusions and recommendations. The thesis is organized from the general to specific and the more specific the subject is, the more detailed it is explained.

1.1 Background

Tomography is a technique to view the internal structure (i.e. density distribution) of an object by scanning it through penetrating waves. A range of tomographic imaging modalities are available depending on the physical phenomena (e.g. X-rays, gamma rays, radio-frequency waves etc.) used. Even its most famous applications (e.g. CT, SPECT, MRI etc.) are used in medical imaging, it is also employed in the other scientific fields such as material science, geophysics and microbiology.

From the etymological point of view, the word *tomography* is derived from two Greek words $\tau\acute{o}\mu o\varsigma$ tomos, meaning *slice* and $\gamma\rho\acute{\alpha}\varphi\omega$ grapho, meaning *to write*. Tomographic imaging basically deals with the reconstruction of cross-sectional images of an object from its projections. Projection measurements, which are acquired from a range of angles, actually corresponds to the line integrals of the image for a set of lines along a range of directions. The primitive reconstruction problem, which asks how to

Figure 1.1: *"Hand mit Ringen (Hand with Rings)"* the first medical X-ray picture by *Wilhelm Röntgen* (1845–1923), it shows the hand of his wife.

determine a function from its available line integrals in mathematical point of view, was solved by Austrian Radon, in 1917. After nearly fifty years of it, both Allan MacLeod Cormack and Godfrey Newbold Hounsfield developed Radon's inverse transformation further and then, Hounsfield experimented his technique using X-rays for projections and computers for calculations. It was the invention of X-ray computed tomography (CT), introduced in 1971. For more details about the history of CT, the reader is referred to [2].

CT scans an object with X-rays sent from different angles and acquires several projections, which are practically the measures of the radiation attenuated by the density of the object. Measured projections, referred as *sinogram*, are then used to obtain the three-dimensional image of the object, which is also considered to be a series of two-dimensional slices. Slice reconstruction is a transformation of the one-dimensional projection measurements from sinogram domain to image domain. In this thesis, our interest is restricted with the reconstruction of the slice images without extending it to the third dimension.

Slice reconstruction problem is solved either analytically or iteratively (e.g. algebraic techniques), by considering the slice image as a function to be reconstructed from its line integrals [3]. Analytical methods, such as Filtered Backprojection (FBP), are

based on Fourier analysis, in particular central slice theorem, and derives the function from an almost complete projection data set. However, in many practical applications of CT, acquired projection data is fewer due to the limitation of radiation dose, time and physical facilities. Iterative methods, even primitive Kaczmarz's method (see Chapter 2), have the ability of reconstructing the function from fewer projections, but their computational cost is higher than the analytical methods, performed in frequency domain. The phrase *iterative reconstruction techniques*, which constitutes the broadest scope of this thesis, is used to denote all algorithms which approximate the solution by iteratively updating the variables. One subcategory of the iterative methods, called as algebraic reconstruction methods (ARM), proposes an algebraic approach to solve the reconstruction problem. The abbreviation ARM is used to refer the algebraic reconstruction algorithms whose principle method is Kaczmarz's [4] (e.g. ART, SART, SIRT), in this document.

Reconstruction problem can be set up as a linear system of equations in which the slice image is taken as an array of unknowns to be evaluated from the available projections. This approach constitutes the basis of the algebraic methods. Several investigations on algebraic methods basically concern with two problems: how to reduce the complexity and how to develop the ability of reconstruction from small number of projections further. The field called discrete tomography is fundamentally focus on the second goal. Discrete tomography techniques (DT) highly reduces the number of required projections by assuming that, the range of the image is restricted to be a discrete set of numbers. There is another recent approach, known as Compressed Sensing (CS) based reconstruction techniques, sharing the same goal with DT. CS based techniques deals with the *compressible* signals (e.g. sparse images) and based on the fundamental fact that the signals can be recovered from very few measurements if the sparsity is the case.

Discrete Algebraic Reconstruction Technique (DART) refers to a novel algorithm, proposed by Batenburg and Sijbers in [5], and lies at the core of this thesis. It basically combines two alternating stages: a continuous iterative reconstruction algorithm and a discretization procedure. In this work, the two stages of DART are separately examined and extended with certain approaches in an effort to improve the reconstruction quality in a time efficient manner. This work first concentrates on the initial guess to make

it easier to segment. This is achieved by a total variation minimization technique (TvMin) instead of algebraic reconstruction method (abbreviated ARM), used in DART. TvMin is a CS based technique, not an algorithm, used to solve ill-posed problems by assuming that a sparse representation of the image exists. Second focus of this thesis is the accurate and efficient discretization of the continuous image, using the projection error and total variation (TV). And as a final interest, the thesis focus on the gray level estimation and reformulate the procedure in order to compute the gray levels, used in discretization stage, in case lack of prior knowledge.

1.2 Literature Review

There are a variety of iterative methods to solve the reconstruction problem by modelling it as a system of linear equations, in which the image has a range of real numbers. The name Algebraic Reconstruction Technique and the abbreviation ART were first used by Gordon, Bender and Herman in 1970 [6]. The technique was applying the Kaczmarz's algorithm (Stefan Kaczmarz, 1937), used to solve linear systems, to the field of image reconstruction. Hounsfield's CT was also using the same principle, so it is possible to say that the ART is the first technique used for the purpose of tomographic imaging. In order to improve the computational inefficiency of the ART or tackle with the noise, it is developed further [7] [8] [9] and it is reproduced as Simultaneous Iterative Reconstructive Technique (SIRT), Simultaneous Algebraic Reconstruction Technique (SART) [10] and so on.

Even though the term discrete tomography (DT) was first suggested by Larry Shepp, in 1994; the discussions on the problems, subjected to DT, goes back to the late 1950s [1]. There are many strategies used to solve DT problems, such as handling the problem as a combinatorial problem [11] [12], approximating the solution statistically (e.g. maximum a posteriori probability estimate (MAP estimate)) by fitting the problem to a probability distribution [13] or combining a continuous reconstruction technique with a discretization step [5]. For a very detailed source on the history of DT, [1] is referred.

Discrete Algebraic Reconstruction Technique (DART) was proposed by Batenburg and Sijbers in [14], described in [5] and then became a well-known reconstruction technique used in the field of DT. It alternates between two stages, one is a continuous ARM and the other is the discretization step by exploiting the prior knowledge on

the gray levels (i.e. the number of gray levels and the values of them). In DART algorithm the discretization is applied during the reconstruction. The discretization of the continuous tomogram is considered as an image segmentation problem. Tomographic image segmentation are usually performed by using global or local thresholding methods to select optimal thresholds by optimizing an objective, such as within/between-class variance, entropy, probability distribution, etc. They all differ in the segmentation accuracy, the computational complexity and the requirements. The original DART [5] uses Otsu's global thresholding scheme [15] which is a histogram-based method described in Chapter 4. However, the only information used by Otsu's algorithm is based on the reconstructed image, whereas there are available projection measurements in a reconstruction problem to be used. On the other hand, the drawback of Otsu type thresholding schemes is its susceptibility to segment the artefacts caused by the reconstruction process. Due to these reasons; Batenburg and Sijbers, the developers of the DART, proposed a thresholding technique, called as Projection Distance Minimization (PDM) in [16], which exploits the available projections. Their method aims to minimize the Euclidean distance between the measured data and the forward projection of the reconstructed tomogram. In [17], they extended the original DART algorithm with PDM segmentation technique, but this time they used PDM approach to determine not only the thresholds, but also the gray levels automatically.

Image reconstruction from small number of projections has received considerable attention among the tomographic imaging scientists. Similar to DT, compressed sensing (or compressive sensing) based methods are also used to accomplish this goal. Compressed sensing (CS) theory [18] deals with the sparse (*compressible*) representations of signals, or images in our case, and states that it is possible to reconstruct them from their fewer number of projections than required according to the Nyquist - Shannon sampling criteria [19]. Computing the sparsest solution directly has high computational load, hence the solution is usually approximated by heuristic methods, that might be roughly classified as greedy algorithms, $\ell_1 - minimization$ and total variation minimization (TvMin). Norm-minimization techniques are used in many applications related to the topic, such as the reconstruction of magnetic resonance images (MRI) [20] since it requires short scan time causing undersampled

projection data. For an image reconstruction problem, image is not sparse in spatial domain, hence the sparsity in another domain is exploited. TvMin uses the norm of gradient of the image, since the gradient is almost always sparse. The application of TvMin concept to image processing is first introduced in [21] and then, the methodology is discussed in [22] [23] [24]. TvMin techniques are often used in medical imaging [25] [26] [27]. A novel comparison between norm-minimizing reconstruction and TvMin is presented in [28] by considering the real world applications.

1.3 Hypothesis

DART utilizes an ARM in order to obtain an initial reconstruction and keeps using it in subsequent iterations, while updating the discretization points (i.e. pixels). Keeping the update procedure as it is, but switching the initial phase with a TvMin step can yield a better approximation, since TvMin technique is good at reconstructing edge-preserved, leading easy-to-segment, images. And what's more, TvMin has the ability of reconstructing from fewer number of projections compared to ARM and that makes it preferable as the initial stage where the system is more under-determined than the succeeding iterations. Even though the TvMin solvers have more computational load than ARM algorithms, it is negligible for a stage, which is performed once and with a small number of iterations.

Discretization of the continuous tomograms is handled by a segmentation, in particular thresholding, method. Using a thresholding scheme which is only based upon the image without considering the available measurements, may not satisfy a true reconstruction; since the input image is actually the output of the former reconstruction and it might be corrupted by different kinds of artefacts. On the other hand, selection of an optimal threshold value, such that minimizes the error in sinogram domain, is a optimization problem with large search space and high computational load, due to its non-differentiability. To reduce the size of search space, this optimization procedure can be combined with an optimized, histogram-based, multilevel, global thresholding method (two-stage multilevel Otsu is used in this thesis). The histogram-based method might first be used to obtain a set of candidate thresholds and then, the optimum threshold can be selected by computing and comparing the forward projections of

each possible segmentations. Here the cost function can also be regularized by using total variation minimization approach, again due to its capability of preserving high frequency details.

Gray level estimation is also considered within the scope of this thesis. In case the gray levels are not known *a priori*, they might be approximated automatically by minimizing the projection error. Since the projection error is differentiable to the gray levels, it can directly be formulated, as it is done in Chapter 4, and used to update the previous gray levels in each subsequent iterations.

2. TOMOGRAPHIC RECONSTRUCTION

2.1 Problem Definition

The physical phenomena behind the projection data acquisition process in CT is the attenuated X-rays. X-rays are sent through the cross section of the scanned object and some of the photons are absorbed, so the ray is attenuated until it reaches the corresponding detector. The amount of the attenuation depends on the density (or attenuation coefficient) of the object and this relationship is described as follows:

$$I_s = I_0 e^{-(\int_0^s f(x)dx)} \tag{2.1}$$

where I_0 is the intensity of the ray while it is passing into the object, I_s is the intensity of the ray while it is passing out from the object and $f(x)$ is the attenuation as a function of the density (so the grayness of the pixels) of the object. By taking the logarithm of both sides, one obtains:

$$\ln(\frac{I_s}{I_0}) = -(\int_0^s f(x)dx). \tag{2.2}$$

The result given in Eq. 2.2 is the mathematical expression of the term *projection*. It is nothing more than the sum of the densities (line integral or ray sum, when using the phrase for an image instead of object) along a line.

The data collection process can be considered as a transform from a two-dimensional slice of the object to one-dimensional projections. An illustration is given in Fig. 2.1. In this section, the attenuation function of the object is denoted by $f(x,y)$. By assuming the rays sent from an angle are all parallel (known as *parallel beam geometry*), the projection for the angle θ, using the normal equation of a line, is given by:

$$b_\theta(s) = \int_{xcos(\theta)+ysin(\theta)=s} f(x,y)dt. \tag{2.3}$$

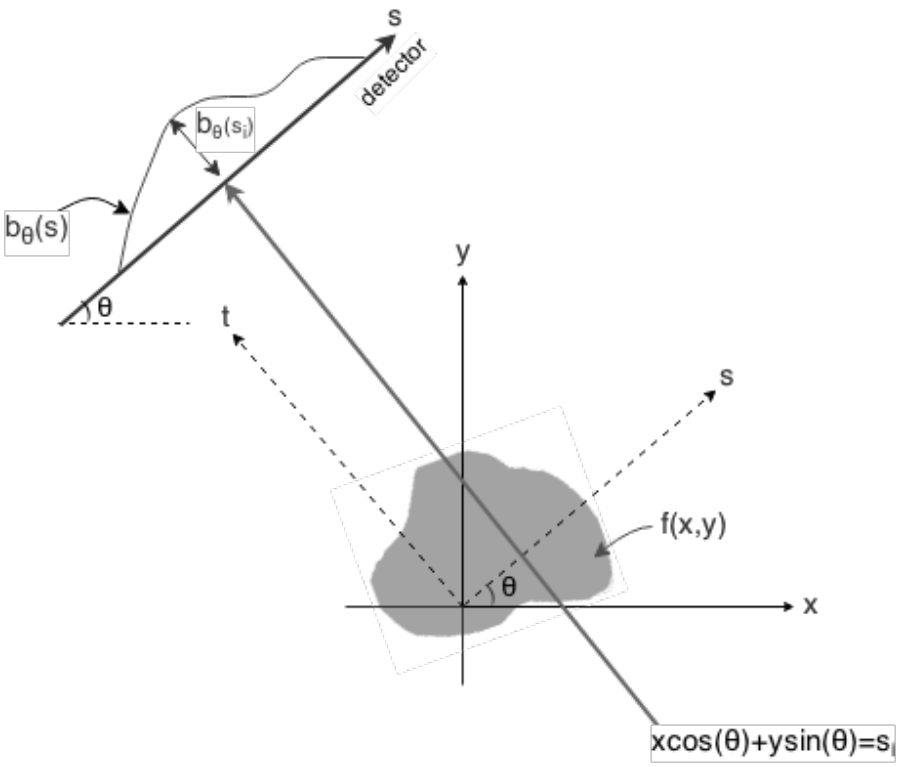

Figure 2.1: The coordinate system of data collection from the projection angle θ using parallel beam geometry.

where s is any ray sent with the angle θ. Eq. 2.3 can also be written as follows:

$$b_\theta(s) = \int_{-\infty}^{\infty}\int_{-\infty}^{\infty} f(x,y)\delta(xcos(\theta)+ysin(\theta)-s)dxdy. \quad \textbf{(2.4)}$$

where δ denotes Dirac-delta function. Eq. 2.4 is the Radon transform of $f(x,y)$, which defines transforms a cross-section of the object from spatial domain to the projection domain where the slice is defined by its line integrals. Projection domain is also called as *sinogram* domain due to the shape of projections. In Fig. 2.2, Radon transform of an example image is shown.

After collecting projection data, the next step is re-transforming it to obtain (the image of) the original slice. At that point, various algorithms are available to reconstruct the data collected. In this thesis, these algorithms are categorized as analytical and iterative, according to the way they are solving the reconstruction problem.

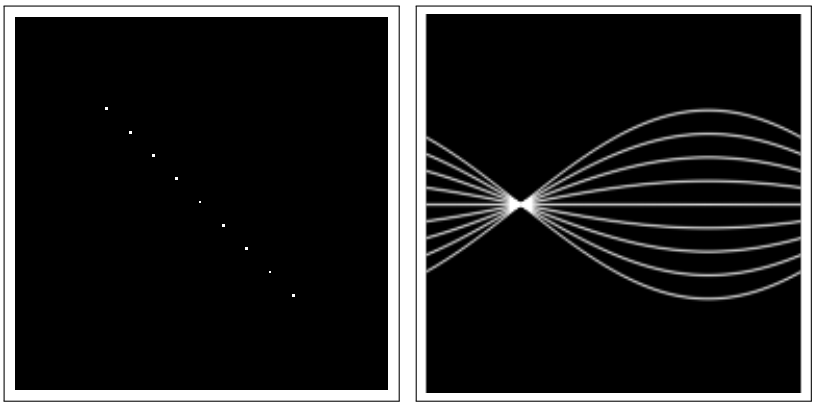

(a) (b)

Figure 2.2: An example on Radon transform: (a) the original image, (b) the sinogram of the image.

2.2 Analytical Reconstruction Techniques

Analytical methods basically solve the reconstruction problem using Fourier transform of the image and its projections. The filtered backprojection (FBP) method is a well-known analytical reconstruction technique. Before making a brief explanation on FBP, the terminology is merely introduced.

Obtaining the projections of an object is modelled as a forward Radon transform in previous section. The *central slice theorem* provides a relationship between the object and the projections, by using Fourier transform. It states that the Fourier transform of the cross-sectional object is approximated by the Fourier transforms of the projections (acquired using parallel beams) at from different angles over 180 degree range. Each transformed projection corresponds to a slice (a line at corresponding angle) of the transformed cross-sectional object (or image).

The Fourier transform of the projection $b_\theta(s)$ is

$$B_\theta(\omega) = \int_{-\infty}^{\infty} b(s) e^{-2\pi\omega s j} ds \tag{2.5}$$

where ω frequency, and the Fourier transform of the object function $F(u,v)$ is given,

$$F(u,v) = \int_{-\infty}^{\infty}\int_{-\infty}^{\infty} f(x,y) e^{-2\pi(ux+vy)j} dxdy \tag{2.6}$$

where $u = \omega cos\theta$ and $v = \omega sin\theta$. So, according to the theorem $B_\theta(\omega)$ is placed along a line at an angle θ in $F(u,v)$. When the possible slices in frequency domain are filled, an inverse Fourier transform can be applied to obtain the image.

2.2.1 Filtered backprojection (FBP)

As it is mentioned in the previous section, Fourier transform of each acquired projection constructs one slice of the Fourier transform of the image, moreover number of the projections are always finite, yielding missing frequencies, especially the higher ones. Lack of information occurs in the high frequency regions, placed away from the origin, since the distance between slices are increasing radially in the frequency domain; and this causes blurry reconstructions. This problem can be handled by interpolation using a rectangular grid in frequency domain.

The FBP method is based on central slice theorem. To tackle with the problem caused by the finite number of projections, it first multiplies the Fourier transforms of the projections with a weight function $|\omega|$ to compensate the increasing distance between the slices, then convolves the image with the weighted backprojections in the spatial domain, instead of interpolating in frequency domain.

$$f(x,y) = \int_0^\pi d\theta \int_{-\infty}^{\infty} B_\theta(\omega)|\omega| e^{2\pi\omega s j} d\omega \tag{2.7}$$

The considerable advantage of FBP is its computational load. Its computational cost is less that the iterative methods, not only due to the analytical nature (single iteration) of it, but also not to need to wait until all projections are collected, to start computation. Moreover, FBP doesn't produce good reconstructions for imperfect (e.g. incomplete, noisy) projections.

2.3 Iterative Reconstruction Techniques (IRT)

Iterative reconstruction techniques refers to the techniques which solve the reconstruction problem iteratively, as the name suggests. These techniques are better in terms of the reconstruction quality, especially under some constraints; but they are computationally more expensive than the analytical methods. The core idea behind

the iterative methods is correction of the solution in each iteration such that a better approximation is satisfied.

2.3.1 Algebraic reconstruction methods (ARM)

Algebraic reconstruction methods assume that the image is an array of unknowns and the reconstruction problem can be set up as a system of linear equations. The unknowns of this system are approximated with respect to the ray sums, iteratively [29]. In each iteration, current reconstruction is re-projected and updated according to how much it satisfies the projection measurements.

$$Ax = b \tag{2.8}$$

where $x \in \Re^n$, the vector of unknowns, represents the image and $A \in \Re^{mxn}$ is the *projection matrix* whose entry a_{ij} corresponds to the weight of the contribution of the pixel x_j to the projection b_i where $b \in \Re^m$.

Eq. 2.8 can be written as weighted sums of the pixels, i.e. the line integrals of rays over the traversed pixels as

$$\sum_{j=1}^{n} a_{ij}x_j = b_i, \quad i = 1,2,\cdots,m \tag{2.9}$$

In practice, $m < n$ and thus Eq. 2.8 is an under-determined system where the solution is not unique, if it exists.

In Fig. 2.3, an illustration is shown to clarify the image projection problem. An n-element square grid is superimposed on the image, in which each element corresponds a discretization point (i.e. pixels). Pixel intensity is uniform within each discretization point x_j. A ray is represented by a thick line (or region between two lines) and the shaded area, which is the intersection of the i^{th} ray and the j^{th} pixel, is the weight a_{ij} for the pixel x_j to the projection measurement b_i.

2.3.1.1 Algebraic reconstruction technique (ART)

Kaczmarz's method, which constitutes the principle of the ARM algorithms (e.g. ART, SART, SIRT), is an iterative projection technique used to solve inverse problems (e.g. image reconstruction), declared as a linear system of equations (e.g. Eq. 2.10). The method is based upon the assumption that x is a point in n dimensional space and the

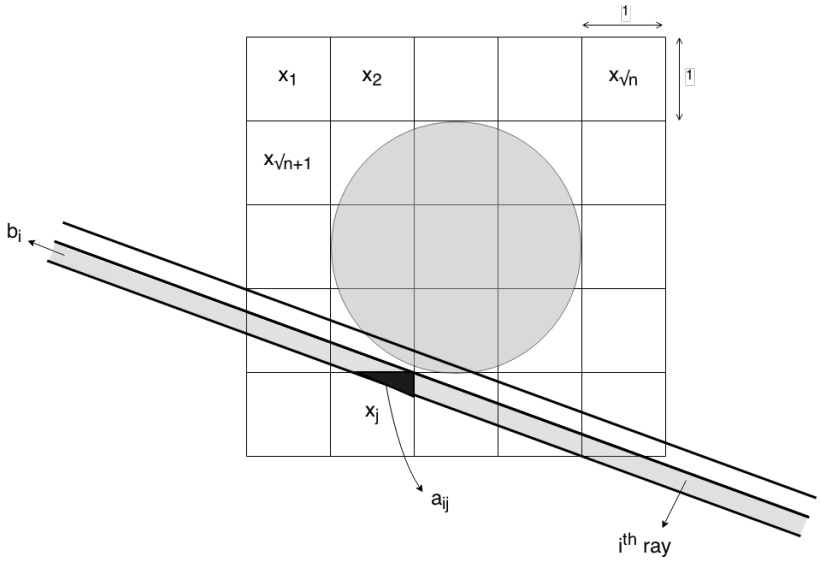

Figure 2.3: An illustration how ART defines the image as an array of unknowns and uses the line integrals of rays.

solution, if exists, corresponds to the intersection of m hyperplanes. These hyperplanes are expressed with the equations of the following linear system:

$$\begin{aligned} a_{11}x_1 + a_{12}x_2 + \ldots + a_{1n}x_n &= b_1 \\ a_{21}x_1 + a_{22}x_2 + \ldots + a_{2n}x_n &= b_2 \\ &\vdots \\ a_{m1}x_1 + a_{m2}x_2 + \ldots + a_{mn}x_n &= b_m \end{aligned} \tag{2.10}$$

What the Kaczmarz's method does is back-projection of the difference between the projection data and the forward projection of the current reconstruction, hereafter the *residual*, on the currently estimated image. It starts with an initial guess x^0 and computes x^1 by projecting x^0 onto the first hyperplane in Eq. 2.10. An illustration of the process is given in Fig. 2.4, for the case of two variables and two hyperplanes. The *update* procedure (or error correction) of the Kaczmarz's method is given in Eq. 2.11.

$$\vec{x}^{(k)} = \vec{x}^{(k-1)} + \lambda \frac{b_i - \vec{a}_i \vec{x}^{(k-1)}}{\|\vec{a}_i\|^2} \vec{a}_i \tag{2.11}$$

where $\vec{a}_i = (a_{i1}, a_{i2}, ..., a_{in})$ is i^{th} row of the projection matrix and λ is the *relaxation parameter*. Relaxation parameter was fixed to $\lambda = 1.$ in Kaczmarz method. $\|\vec{a}_i\|^2$ is the normalization factor. In Eq. 2.11, the update is performed for each projection measurement b_i separately meaning that the k^{th} iteration consists of a *sweep* through

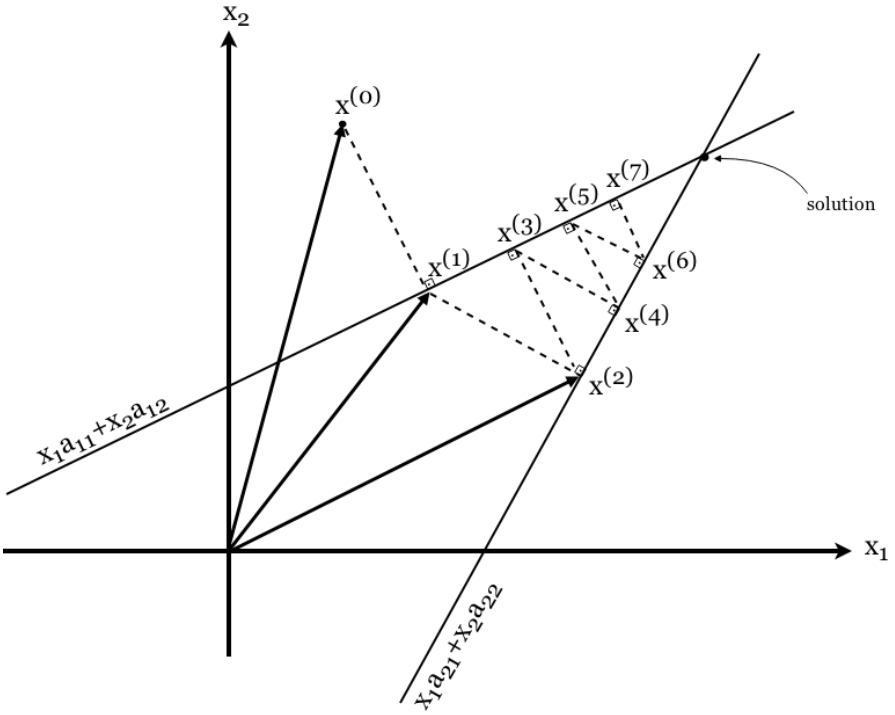

Figure 2.4: A geometric illustration on the re-projection principle of ARM using the Kaczmarz method in case of two unknowns and $\lambda = 1$.

the m projection measurements. The algorithm iterates through the equations periodically, as so $i = (i-1)\ mod\ (m) + 1$.

Algebraic Reconstruction Technique (ART) is a rediscovery of the Kaczmarz's method to be used in tomographic image reconstruction field. It updates x by using Eq. 2.11 until it converges. Here the converge refers to the case where a termination criterion, such that the residual $r = b - Ax^k$ is smaller than a threshold, is met.

2.3.1.2 Simultaneous iterative reconstruction technique (SIRT)

The ART algorithm updates the image vector per ray, such that the update satisfies only a single equation representing the corresponding ray integral. The SIRT algorithm, on the contrary, updates the image vector after all equations are considered. The update procedure of SIRT is given in Eq. 2.12 according to [30].

$$\vec{x}^{(k)} = \vec{x}^{(k-1)} + \lambda \frac{1}{\sum_i^m a_{ij}} \sum_i^m a_{ij} \frac{b_i - \vec{a}_i \vec{x}^{(k-1)}}{\sum_{j=1}^n a_{ij}} \tag{2.12}$$

The iterative procedure given in Eq. 2.12 aims to find a solution which minimizes the weighted squared projection error $\|Ax-b\|_R = (Ax-b)^T R(Ax-b)$ where $R \in \mathbb{R}^{mxm}$ is diagonal matrix that contains $r_i i = \frac{1}{\sum_j a_{ij}}$ [30].

2.3.1.3 Simultaneous algebraic reconstruction technique (SART)

The SART algorithm [10] is proposed as a combination of the ART and the SIRT algorithms. It updates superior implementation of ART and based on a simultaneous update of the current reconstruction, just like SIRT. In the SART algorithm, the update procedure is applied for all rays in a given scan direction (projection) instead of each ray separately as in the conventional ART or instead of all rays simultaneously as in the SIRT. The SART update is given by:

$$\vec{x}^{(k)} = \vec{x}^{(k-1)} + \lambda \frac{1}{\sum_{i \in \Omega_t} a_{ij}} \sum_{i \in \Omega_t} a_{ij} \frac{b_i - \vec{a}_i \vec{x}^{(k-1)}}{\sum_{j=1}^{n} a_{ij}} \tag{2.13}$$

where Ω_t is the set of indices of the rays sent from t^{th} projection direction. Eq. 2.13 starts with an initial estimate x^0 and updates each estimate with a new one, iteratively. When all projection directions are swept, one SART iteration is accomplished.

ART is good at rapid converge, but it results with a noisy looking reconstruction. On the other hand, SIRT exhibits smoother reconstructions but it requires larger number of iterations to converge. SART aims to tackle with the noise, caused by the sequential update approach of ART, by proposing a SIRT-type algorithm; but it also aims to reduce the cost of SIRT by considering a subset of equations in the system Eq. 2.10. The proof and details on how this objective is satisfied by SART are accounted in [10], the original paper of the SART algorithm.

3. RECONSTRUCTION FROM SMALL NUMBER OF PROJECTIONS

3.1 Problem Definition

The name of this chapter is inspired from the name of the paper [28], proposed by Herman and Davidi, in 2008. The reason having a chapter with this name is a need to group *discrete tomography* and *compressed sensing* topics, since both are directly related to the proposed method, in an appropriate place within entire document.

Reducing the number of projections have a crucial meaning in tomographic reconstruction field. In many applications of CT, one desires to limit the radiation dose due to the fact that it can damage to the exposed structure. To do that, the number of X-ray projections which are acquired by the detectors should be reduced. Besides, there are often limitations about the physical facilities and required time, which prevents to acquire large number of projections. However, the image reconstruction problem suffers from the difficulty that there are multiple images having identical projections [28] when the number of projections small. Taking an algebraic viewpoint, this difficulty is due to the under-determined characteristic of the system (see Chapter 2). Nyquist-Shannon sampling theorem states that a perfect reconstruction of the signal is possible if the sampling rate is at least two times of the highest frequency of the signal. If one has prior knowledge on the frequencies, the reconstruction can be accomplished using fewer measurements. Both of the fields discrete tomography and compressed sensing aims to reconstruct desirable images from even fewer number of projections (incomplete) than required by the Nyquist-Shannon criterion and they both make some assumptions to accomplish this goal.

3.2 Discrete Tomograhy

The name "discrete tomography" was suggested by Larry Shepp, who organized the meeting, named DIMACS Mini-Symposium on Discrete Tomography, in 1994. The problems related to this topic had been considered as combinatorial problems until

they are grouped with this name after subjected meeting, and then new approaches rather than combinatorial ones were started to be proposed. Discrete tomography (DT) basically assumes that the range of the function, which will be reconstructed, is known to be a given discrete set [1]. Let $\Xi^L = \{\xi_1, \xi_2, .., \xi_L\}$ be *a priori* discrete set with L elements, each of which, $\xi_l \in \mathbb{Z}^L$, is corresponding to a gray level (label) for an image reconstruction problem. This reconstruction problem of discrete tomography is formulated as follows:

$$find \quad Ax = b, \quad such \quad that \quad x \in \{\xi_1, \xi_2, .., \xi_L\} \tag{3.1}$$

There are roughly two variants of discrete tomography. They differ from each other in terms of the domains of the functions (images in our case). First approach basically deals with the reconstruction of finite subset of the integer *lattice*. In [1], Herman and Kuba define an image, considered by DT, as a function $x : F \to \{\xi_1, \xi_2, .., \xi_L\}$, where F is a subset of $\mathbb{Z}^n$, meaning that an integer lattice in n dimensional space and the gray levels of each of the lattice points must be equal to the one of the $\xi_l \in \Xi^L$ [31]. For this first approach, by assuming κ is a set of lines that intersects F, the projection, line sums (i.e. ray sums) of the function x, is defined as:

$$\sum_{t \in F \cap \ell} x(t), \quad \ell \in \kappa \tag{3.2}$$

In Fig. 3.1, a simplified problem by taking only binary images into consideration, so the label set is restricted with the values $\Xi^2 = \{0, 1\}$, illustrated together with corresponding linear system, in order to exemplify the first approach which assumes the domain of the function is also discrete.

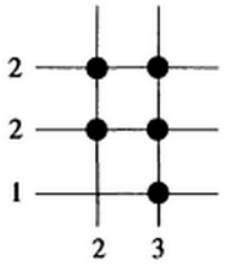

$$\begin{array}{rcccccl} x_1 & +x_2 & & & & & = 2 \\ & & x_3 & +x_4 & & & = 2 \\ & & & & x_5 & +x_6 & = 1 \\ x_1 & & +x_3 & & +x_5 & & = 2 \\ & x_2 & & +x_4 & & +x_6 & = 3 \end{array}$$

Figure 3.1: A lattice set of $\mathbb{Z}^2$, its projections in two directions and corresponding system of linear equations [1]

In contrast to the first variant which uses integer valued functions, second approach assumes that the image has a continuous domain (such as Euclidean space), $x : \mathbb{R}^2 \to \{\xi_1, \xi_2, .., \xi_L\}$, while it has a finite and discrete set of range [31].

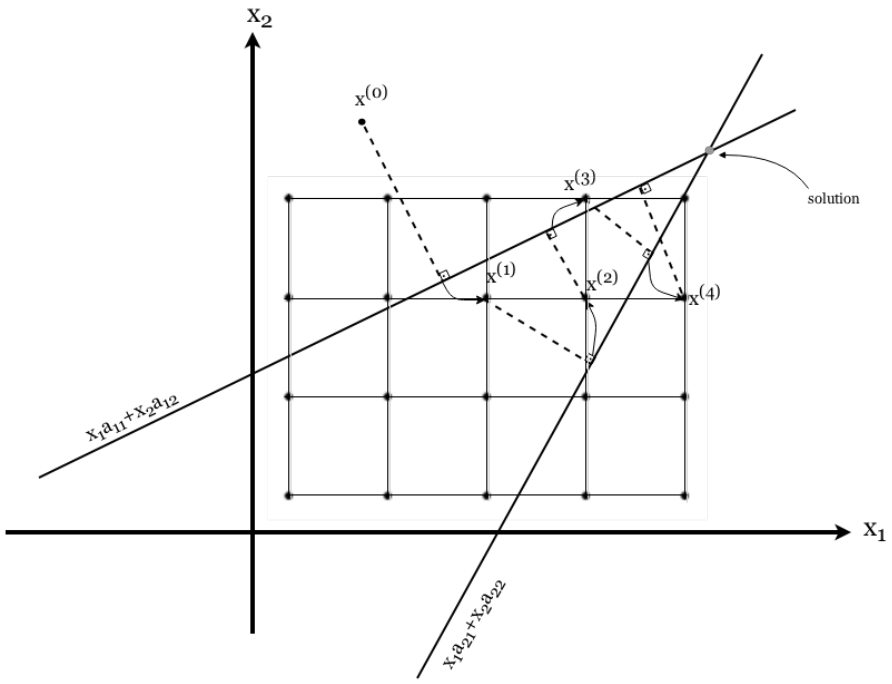

Figure 3.2: A geometric illustration for a discrete reconstruction using one iteration continuous reconstruction followed by discretization.

DT researchers try to answer the questions such that, is there a solution consistent with the observed projections; is it unique, if a solution exists and how the solution is reconstructed. There are different strategies to answer and solve these questions, for both variants of DT. The problem is sometimes redefined as a combinatorial problem (e.g. a network flow problem [11] [12]), sometimes modelled by fitting a probability distribution or sometimes solved using optimization techniques. The continuous algebraic reconstruction techniques can also be exploited while solving a DT problem. The Discrete Algebraic Reconstruction Technique (DART) algorithm, which is lying at the core of this study, also uses a continuous algebraic reconstruction method to reconstruct the image. It applies the discretization after the continuous reconstruction by using an image segmentation technique to enforce the range being discrete and finite. DART algorithm is discussed in Chapter 4, in detail.

3.3 Compressed Sensing Theory

The field of compressed sensing (CS) was pioneered by Donoho in [18] and by Candès et al. in [19], in 2006. The idea behind the field of compressed sensing is to recover a sparse (i.e. having very few non-zero coefficients) signal from very few linear measurements. Here the assumption is having a sparse $x \in \mathbb{R}^n$ to be reconstructed from the observations (projection measurements in our case) formulated as follows.

$$b = Ax \tag{3.3}$$

For a sparse recovery problem, the objective is finding the sparsest solution and to accomplish this goal one should first know how the sparsity is measured. Minimization of the number of non-zero coefficients is corresponding to the $\ell_0 - minimization$ technique, formulated in Eq. 3.4, which is the most primitive way and unfortunately, it is an NP-hard problem.

$$\min_x \|x\|_0 \quad s.t. \quad Ax = b \tag{3.4}$$

where $\|x\|_0$ is defined as follows:

$$\|x\|_0 := \#\{j : x_j \neq 0\} \tag{3.5}$$

After it was discovered that $\ell_0 - minimization$ is same with $\ell_1 - minimization$, which is the closest convex norm, under some conditions [32], solving such an NP-hard problem has become possible [33]. So the $\ell_1 - minimization$, which is also known as *Basis Pursuit*, problem is formulated as in Eq. 3.6.

$$\min_x \|x\|_1 \quad s.t. \quad Ax = b \tag{3.6}$$

where $\|x\|_1 = \sum_j |x_j|$. By considering that the projections are noisy as in the following model:

$$b = Ax + e \tag{3.7}$$

where e is the error term with bounded energy $\|e\|_2^2 \leqslant \varepsilon$, the $\ell_1 - minimization$ problem should be redefined as follows:

$$\min_x \|x\|_1 \quad s.t. \quad \|Ax - b\|_2^2 \leqslant \varepsilon \tag{3.8}$$

where $\varepsilon > 0$ is controlling the consistency.

The same problem can also be written as an unconstrained optimization problem as in Eq. 3.9.

$$\min_x \frac{1}{2}\|Ax-b\|_2^2 + \mu\|x\|_1 \tag{3.9}$$

where μ is the *regularization parameter*. This parameter is indicating the importance of each terms. Since it has a crucial meaning, there are various studies on selecting the appropriate regularization parameter.

Typically, in an image reconstruction problem, signals are not themselves sparse but they might be sparse in an appropriate transform domain, with some orthonormal basis Φ, such that $x = \Phi c$ where c is sparse. If almost all the entries of c are zero (or almost zero), x is said to be sparse in Φ domain. So the problem is formulated as in Eq. 3.10 so that c is desired to be recovered from the observations, defined as follows:

$$\min_x \|c\|_1 \quad s.t. \quad A\Phi c = b \tag{3.10}$$

Most of the CT images, have large amount of low frequency (smooth) regions while having fewer high frequency ones. So, transforming an image to frequency domain will probably result with a sparse representation of it, due to the coefficients which are very close to zero. Fourier, Wavelet and discrete cosine transform are all used as sparsifying transforms. On the other hand, the signals may have sparser representations even in spatial domain. Using the spatial finite differences, using first or second derivations (e.g. Laplacian transform) may yield better results, since the gradients of the images are generally sparse. Total variation minimization (TvMin) is a well-known technique which exploits the sparsity of the gradient magnitude of the image and tries to minimize the total variation (TV) which denotes the $\ell_1 - norm$ of the gradient magnitude. The problem can be defined as follows:

$$\min_x TV(x) \quad s.t. \quad \|Ax-b\|_2^2 \leqslant \varepsilon \tag{3.11}$$

where $TV(x)$ denotes the total variation of the image and $\|Ax-b\|_2^2 \leqslant \varepsilon$ enforces the measured data consistency.

The standard TvMin techniques solve the following unconstrained formulation of the problem:

$$\min_{x} TV(x) + \frac{\mu}{2}\|Ax - b\|_2^2 \qquad \textbf{(3.12)}$$

TvMin techniques are known as edge-preserving methods, which yields sharper reconstructions. TV regularization is also applied on image denoising and deconvolution problems. For more details on TvMin technique, one is referred to Chapter 4 of this document.

4. PROPOSED METHOD

The proposed method involves three major parts: (1) using TvMin as an initial stage to DART, (2) selection of thresholds, which minimizes the projection error and total variation, from a finite set of candidates obtained a histogram-based segmentation procedure and (3) gray level estimation. In this chapter, first two sections are reserved for the DART algorithm and the TvMin technique, respectively; since the proposed method, is said to be a combination of these two methods.

4.1 Discrete Algebraic Reconstruction Technique (DART)

The DART was first proposed by Batenburg et al. in [14]. DART combines a continuous algebraic reconstruction method (ARM) with a discretization step in order to obtain a discrete image in which all pixels are assigned to one of the gray levels from a pre-defined level set. Discretization step requires a prior knowledge, It is capable of computing better reconstructions from fewer projections as compared to the alternatives, not only because of its discrete nature, but also by reason of its ability to reduce the number of variables by focusing on the regions where the reconstruction procedure is tend to fail. These regions correspond to the boundary pixels on the image and they are tried to be reconstructed with the subsequent iterations, while the others are fixed. Less number of variables makes the problem less under-determined resulting with more accurate solution.

The DART starts with a continuous step to compute an initial approximation by performing fixed number of ARM iterations. After several ARM iterations, a reconstruction whose range is real numbers is obtained. The resulting image tends to have artefacts due to the less number of projection data, limited range of projection angles or noise, and it is hard to detect where the exact boundaries of the object are, from reconstructed image. This step is followed by the segmentation step in which the reconstructed image is discretized, so that it has only the gray values from given level

set: $x_j \in \{\xi_1, \xi_2, .., \xi_L\}$. To segment the image, Otsu's global thresholding scheme is used by choosing the thresholds as the average of two consecutive gray levels.

The segmented image generally has the correct gray levels in the interior regions, which are far away from the boundaries. The DART exploits this observation in order to reduce the number of variables for the subsequent iterations. Hence, the *boundary pixels* B, which differ from at least one of the adjacent pixels using 8-connected neighbourhood, are extracted from the segmented image. Instead, one can use 4-connected neighbourhood which may yield less number of boundary pixels, so the variables, to be updated.

Next, the boundary pixels are extended with a randomized scheme in which a non-boundary pixel is included to the set of B with probability $1 - p$, where p is the *fix probability* and defined as $0 < p \leq 1$. This process is accomplished to cope with the images with small holes and the noisy projections. This extended new set is called as *free pixels* U which implies the only pixels that will be reconstructed in the next iteration of DART. The remaining pixels, called *fixed pixels* and denoted by F, are assigned to the pre-defined gray levels and not updated.

Recall the system of linear equations that is presented in Section 3.2

$$Ax = b \tag{4.1}$$

where $A \in \mathbb{R}^{mxn}$ is the *projection matrix*, $b \in \mathbb{R}^m$ is the vector of the projection measurements and $x \in \mathbb{R}^n$ is the vector of the image pixels.

Eq. (4.1) consists of m linear equations while it has n variables and the systems considered in tomographic reconstruction mostly be under-determined, i.e. $n \gg m$, meaning fewer projections than the discretization points (pixels). If the elements of set of F are assigned to the correct gray levels, the remaining less under-determined system yields more accurate results for the pixels $i \in F$. Eq. 4.2 shows how the remaining system is formed when the variable x_i is fixed and removed from the equations.

$$\begin{pmatrix} \vdots & & \vdots & \vdots & & \vdots \\ a_{i,1} & \dots & a_{i,j-1} & a_{i,j-1} & \dots & a_{i,n} \\ \vdots & & \vdots & \vdots & & \vdots \end{pmatrix} \begin{pmatrix} x_1 \\ \vdots \\ x_{j-1} \\ x_{j+1} \\ \vdots \\ x_n \end{pmatrix} = \begin{pmatrix} b_1 \\ \vdots \\ b_m \end{pmatrix}. \tag{4.2}$$

Succeeding ARM steps are performed on the new system where the variables are restricted to be the set of U and the new measured data is the *residual sinogram* $r^k \in \mathbb{R}^m$, which is computed by subtracting the forward projection of the image with the fixed pixels only $f^k \in \mathbb{R}^n$ from the projection data as in Eq. 4.3, where k denotes the DART iteration number.

$$r^k = b - Af^k. \tag{4.3}$$

In Eq. 4.4, a fixed number of ARM update is applied on the free pixels and the resulting reconstruction is added on the already fixed ones.

$$x^{(k+1)} = f^{(k)} + S_{u^{(k)}} r^{(k)}. \tag{4.4}$$

where S denotes the ARM operator which is applied on the residual sinogram $r^{(k)}$ to update the image of update pixels $u^{(k)} \in \mathbb{R}^n$.

As a final stage of one DART iteration, a Gaussian smoothing filter is applied on the resulting image $x^{(k+1)}$ to suppress the fluctuations between the fixed and non-fixed pixels.

DART iterations are performed as long as the termination criterion, such as a fixed number of iterations or converge of *the projection error*, is not met.

DART reduces the number of unknowns in the original under-determined system, since almost each succeeding iteration comes up with the reconstruction problem to be solved for only free pixels. This approach not only reduces the computational cost but also computes higher quality reconstructions.

To clarify the DART algorithm, the pseudo code is given in Fig. 4.1.

Algorith 1 (DART)

$x^{(0)} \longleftarrow ARM(x := 0, A, b), \quad k := 0$

while (*stop criterion is not met*) **do**

begin

Segment image: $s^k \longleftarrow Otsu(x^k)$

Subdivide s^k into free pixels $U^k \subset x^k$ and fixed $F^k = x^k \setminus U^k$

Extend U^k with the pixels in F^k with probability $1-p$

Compute the residual sinogram $r^k \longleftarrow b - Af^k$

Update the image of free pixels $u^k \longleftarrow ARM(u^k, A^k, r^k)$

Smooth u^k and obtain $x^{k+1} \longleftarrow f^k + u^k$

end

Figure 4.1: The pseudo code of the original DART algorithm

The drawback of the original DART algorithm is requiring the gray levels to be known in advance, besides the number of them. In [17], it is shown that, the gray levels can be estimated automatically, while the algorithm is already been performed. Gray level estimation is accomplished with an optimization scheme, whose objective is minimizing the projection distance. Projection distance, used as the *projection error* in the proposed method, refers to the distance between the measured data and the forward projection of the reconstructed image. In [17], the optimization procedure is called as projection distance minimization (PDM), hence the algorithm is named as PDM-DART. The PDM-DART algorithm estimates the segmentation parameters, referring both the gray levels and the threshold values, to be used in segmentation step.

4.2 Total Variation Minimization (TvMin)

Compressed Sensing (CS) theory [18] ensures that it is possible to recover a signal, which is *a priori* known to be sparse (or sparse by a transformation with a known transform), from its far fewer measurements required by Shannon's criterion. Image reconstruction problem can be classified as a compressed sensing problem (CS), since the available measurements are mostly fewer than the variables, resulting with an

under-determined system. There are diverse range of techniques developed to solve CS problems, including total variance (TV) minimization (abbreviated as TvMin in this work) technique which is a generalized form of another well-known $\ell_1 - minimization$ technique.

TV was introduced as a criterion for image denoising and reconstruction in 1992 by Rudin et al., with the motivation of finding an edge preserving method [21]. Basic foundation of the TV regularization methods is the assumption of having sparse gradients (see Fig. 4.2), instead of signals. The discrete gradient of the matrix image X at the pixel at i^{th} row and j^{th} column is denoted by $D(X)_{ij}$ and defined as the magnitude of the horizontal and vertical gradients $D_x(X)_{i,j} = |X_{i+1,j} - X_{i,j}|$ and $D_y(X)_{i,j} = |X_{i,j+1} - X_{i,j}|$, respectively. Eq. 4.5 shows how it is defined for an image X written in matrix notation.

$$D(X)_{i,j} = \sqrt{(D_x(X)_{i,j})^2 + (D_y(X)_{i,j})^2} \tag{4.5}$$

And the total variation $TV(X)$ or $TV(x)$,by rewriting the image in vector notation as x, is defined as the sum of the discrete gradient for each pixel.

$$TV(x) = \|D(x)\|_p = \sum_j |D(x)_j| \tag{4.6}$$

where $D(x)_j$ is the discrete gradient of x at the pixel j, x denotes the image written using vector notation and $\|.\|_p$ is either ℓ_1- or $\ell_2 - norm$, corresponding to anisotropic TV and isotropic TV respectively.

Since the isotropic TV is not differentiable, anisotropic TV, which corresponds to $\ell_1 - norm$, is used and it leads to exploit $\ell_1 - minimization$ techniques, when the sparsity in gradient domain is the case. The TV minimization is a constraint optimization problem, defined as follows:

$$min_{x \in \mathbb{R}^n} \sum_j |D(x)_j|, \quad s.t. \quad Ax = b \tag{4.7}$$

This problem can also be rewritten as an unconstrained problem as follows:

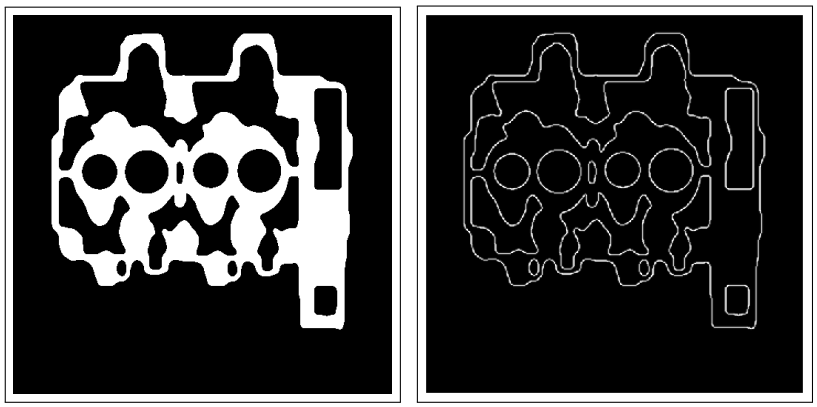

(a) (b)

Figure 4.2: An example on sparse gradients exploited by TV minimization technique (a) the original image, (b) its gradient magnitude.

$$min_{x\in\mathbb{R}^n} \sum_j |D(x)_j| + \frac{\mu}{2}\|b - Ax\|_2^2 \qquad \textbf{(4.8)}$$

where $p = 1$ in most cases and μ is a regularization parameter. Eq. 4.8 aims to minimize both the TV and the *projection error*, simultaneously.

Researches show that the minimization of TV yields sharper reconstructions by preserving the high frequency regions. The significant advantage of the TvMin technique is the ability of recovering non-sparse signals, e.g. almost all of the subjected images, if its gradient is sparse. On the other hand, the technique has disadvantages in terms of computational complexity due to its non-differentiable and non-linear characteristics. To cope with this problem, meaning to solve the problem faster, several algorithms are proposed by either reformulating [34] [35] the problem or splitting it into low-complexity sub-problems, as in [36]. For more detailed presentation of the TV regularization models, the reader is referred to [24] [22].

4.3 The Proposed TvMin+DART Algorithm

The DART algorithm starts with a fixed number of ARM iterations to compute an initial approximation. In the paper of the original DART, published by Batenburg et al., the SART algorithm (discussed in Chapter 2) is used; while the PDM-DART, proposed by Aarle, et al., prefers the SIRT algorithm, instead. In this work, the SART is employed in order to update the free pixels as in the original DART, however the initial stage is switched to another heuristic approach: TvMin. In this section, the proposed algorithm which combines DART with an initial TvMin stage, in order to ensure a

better initial guess, is described. The algorithm also proposes to use an optimized global thresholding scheme by exploiting the valleys in the gray level histogram and aims to minimize both the projection error and the TV simultaneously.

It is important to start DART with a good initial estimate, in terms of the compliance to segmentation. In the proposed algorithm, the initial reconstruction is computed by TvMin, as it is defined in Eq. 4.8, instead of any other ARM (e.g. ART, SART, SIRT). This approach yields a more easy to segment reconstruction to be used in segmentation step, since the artefacts formed after TvMin is less than the SART algorithm, as it can easily be seen from Fig. 4.3. The image computed by TvMin reconstruction is sharper and high frequency regions, such as edges and boundaries, are more accurately preserved. Two initial reconstructions, one from SART and another from TvMin, are shown in Fig. 4.3.

TvMin constrained optimization problem, given in Eq. 4.7, is known having high computational cost due to its non-differentiability and non-linearity. However, it has already been solved in [36] efficiently and named as TV minimization scheme based on augmented Lagrangian and alternating direction algorithms (TVAL3 scheme). This TV solver combines augmented Lagrangian and alternating direction algorithms to be able to optimize TV model. The solver is used to solve Eq. 4.8 with non-negativity constraint, defined as Eq. 4.9, in the proposed method.

$$min_{x\in\mathbb{R}^n} \sum_j \|D(x)_j\|_p + \frac{\mu}{2}\|b-Ax\|_2^2 \quad s.t. \quad x \geq 0, \tag{4.9}$$

where $x \in \mathbb{R}^n$, $D_j x \in \mathbb{R}^2$ is the discrete gradient of x at pixel j, $A \in \mathbb{R}^{mxn}$ is the projection matrix and $b \in \mathbb{R}^m$ is the observation of x with some linear measurements and μ is a regularization parameter used to determine the importance of the data fidelity term. $\|.\|$ is either ℓ_1- or ℓ_2-norm.

The output of the TvMin technique is then used as the initial guess for the succeeding DART algorithm and this process is accomplished in a time efficient manner using TVAL3 solver.

In this work, a thresholding scheme is also proposed to be used in segmentation step of DART, by combining a histogram-based approach with total variation regularization problem. In the proposed thresholding scheme, the thresholds which minimize both

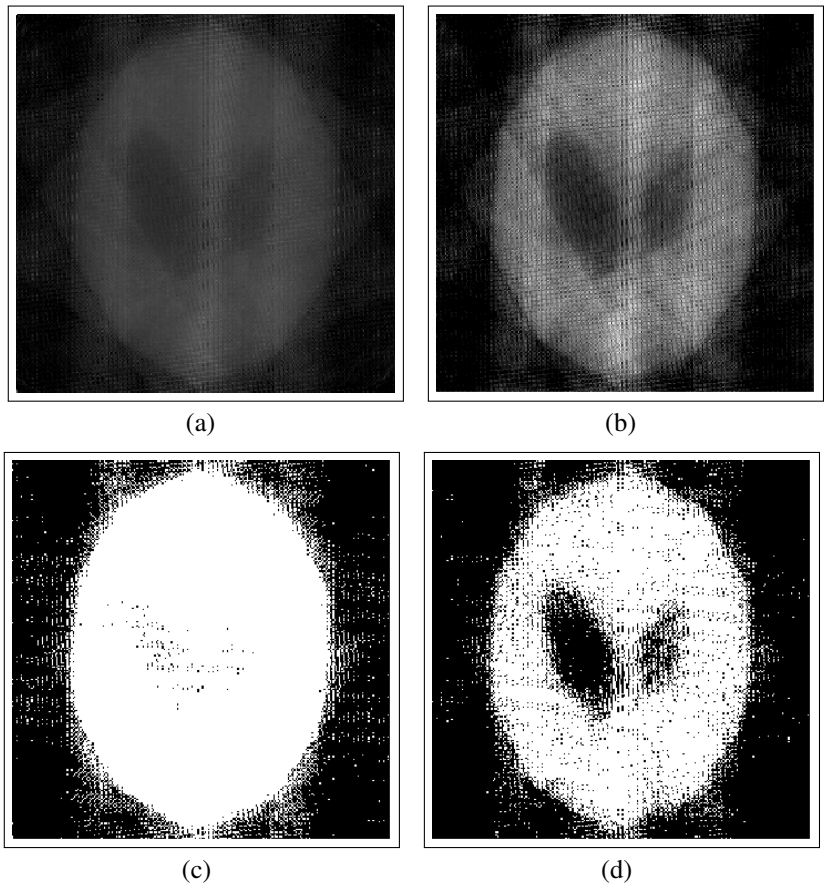

Figure 4.3: Initial reconstructions obtained with $t_0 = 3$ iterations and $p = 7$ number of noisy projections using (a) SART, (b) TvMin and segmented (c) SART, (d) TvMin reconstructions

the projection error and total variation are selected among a number of *candidate thresholds*, obtained by a two-stage multilevel Otsu algorithm (TSMO) [37]. To determine the number of candidate thresholds, a *valley estimation* (VE) procedure, proposed in [37], is utilized. To be able to express the overall scheme; Otsu's global thresholding algorithm and its more efficient two stage extension are explained first.

Otsu's algorithm [15] selects an optimum global threshold by either minimizing within-class, given in Eq. 4.10 or maximizing between-class variance, given in Eq. 4.11 where σ, τ and p denotes the standard deviation, the threshold and the occurrence probability of the associated cluster, respectively. The formulation is first given according to the bi-level thresholding where the idea is finding a threshold to be able to extract the region of interest (foreground) from background. So the associated subscripts f and b, used in the Otsu's formulation, are referring the foreground and background pixels, respectively.

$$\sigma^2_{within}(\tau) = p_f(\tau)\sigma^2_f(\tau) + p_b(\tau)\sigma^2_b(\tau) \qquad \textbf{(4.10)}$$

where $p_{subscript}(\tau) = \frac{n_{subscript}(\tau)}{n}$ using n to denote the total number of pixels and $n_{subscript}$ is the number of the pixels associated with the given *subscript*.

$$\begin{aligned}\sigma^2_{between}(\tau) &= \sigma^2 - \sigma^2_{within}(\tau) \\ &= (\sum_j x_i^2 - \mu^2) - p_f(\tau)(\sum_{j\in f} x_i^2 - \mu_f^2) - p_b(\tau)(\sum_{j\in b} x_i^2 - \mu_b^2) \\ &= p_f(\mu_f - \mu)^2 + p_b(\mu_b - \mu)^2\end{aligned} \tag{4.11}$$

where $\mu_{subscript}$ denotes the mean intensity of the associated *subscript* and μ without *subscript* is the mean intensity of whole image.

Since Otsu's algorithm searches for a threshold τ to maximize Eq. 4.11, the problem can be defined as in Eq. 4.12.

$$\tau^* = \underset{\tau}{\operatorname{argmax}}\{\sigma^2_{between}(\tau) = p_f(\mu_f - \mu)^2 + p_b(\mu_b - \mu)^2\} \tag{4.12}$$

Otsu's bi-level thresholding formulation can straightforwardly be extended to a multilevel thresholding problem by defining the between-class variance of L clusters, as shown in Eq. 4.13.

$$\sigma^2_{between}(T) = \sum_{l=0}^{L-1} p_l \mu_l^2 - \mu^2 \tag{4.13}$$

So, the objective becomes:

$$T^* = \underset{T}{\operatorname{argmax}}\{\sigma^2_{between}(\tau_0, \tau_1, ..., \tau_{L-2}) = \sum_{l=0}^{L-1} p_l \mu_l^2 - \mu^2\} \tag{4.14}$$

where L is the number of gray levels (clusters) leading $L-1$ thresholds and T denotes the threshold vector in which $\tau_l \in T$.

After a brief explanation on Otsu's method, here its more efficient successor two-stage multilevel Otsu's (TSMO) thresholding, proposed by Huang and Wang in [38], is concisely presented. TSMO is, as the name implies, a two-stage Otsu optimization procedure and it utilizes the histogram binning concept to reduce the computational complexity of Otsu. In the first stage of TSMO, the gray level histogram of the input image is divided into K (TSMO uses $K = 32$) bins and assume these bins are clustered into L clusters (from now *bin clusters*), each of which is denoted by C_l, using Otsu's multi-level thresholding scheme. The objective of this stage is maximizing the between-class variance of the bin clusters. The equations Eq. 4.13 and Eq. 4.14 can

easily be redefined by rewriting the terms p_l and μ_l by means of the bin clusters' occurrence probability p_{φ_k} and the mean intensity μ_{φ_k} as follows:

$$p_l = \sum_{\varphi_k \in C_l} p_{\varphi_k}, \quad \mu_l = \sum_{\varphi_k \in C_l} \mu_{\varphi_k} \frac{p_{\varphi_k}}{p_l} \tag{4.15}$$

where $\varphi = \{\varphi_k | k = 1, 2, ..., K\}$ denotes the set of bins, so φ_k is used to indicate k^{th} bin in the histogram.

At the end of the first stage of TSMO, $L-1$ thresholds, corresponding to the bins, are obtained. In the second, and also final, stage, Otsu's bi-level thresholding is used to determine the optimal threshold τ_l^* for each bin φ_k^* obtained from the first stage.

$$\tau_l^* = \underset{\tau_l \in \varphi_k^*}{\operatorname{argmax}} \{\sigma_{between}^2(\tau_l)\} \tag{4.16}$$

To resume on the proposed algorithm, the segmentation step of the original DART is accomplished using Otsu's thresholding algorithm which is a histogram-based method. In PDM-DART, on the contrary, the determination of the threshold values is managed using an optimization scheme, which is not histogram-based, to minimize the projection distance (the norm of the distance between measured projections and the forward projection of the segmentated image). Since PDM-DART aims to estimate the gray levels, together with the optimal thresholds; the projection distance is optimized with respect to both the gray levels and the thresholds. However, the cost function (projection distance) in this problem is not differentiable to the thresholds, so PDM-DART runs a simplex search through all the pixels by computing the forward projection for each. At that point, an approach which limits the search space to a set of candidate thresholds might be reasonable. In this work, these candidates are chosen by utilizing the TSMO approach after determining the number of candidates by counting the valleys in the gray level histogram as in [37].

Histogram valley estimation procedure, used in [37], is proposed as a pre-process to the TSMO algorithm to determine the number clusters. To briefly explain the procedure, first of all the normalized histogram binning is performed by dividing the histogram of the reconstructed image into K (=32) bins, each of which is denoted by ψ_k, containing $|\psi_k| = 8$ pixels as in [37]. Then, normalized histogram H_k of each bin is estimated by using the following equation:

$$H_k = \frac{h_k}{max(h_k)} x100, k \in 0, 1, ..., K-1 \tag{4.17}$$

where $h_k = \sum_{k \in \psi_k} n_k$ and n_k denotes the number of pixels in k^{th} bin.

Next, each group is assigned to a probability according to its location on the histogram and the normalized histogram distribution. This probability estimation stage is performed by scanning the histogram from the lower gray levels to the higher ones and comparing the normalized histogram of the current group with its neighbouring groups. If H_k of current group is less than both of its neighbours, its probability is set to 100%. Otherwise, if H_k is equal to H_{k-1} while less than H_{k+1} or if it is less than H_{k-1} while equal to H_{k+1}, 75% and 25% are assigned as probabilities of being a valley, respectively. For the groups whose normalized histogram is equal to the previous one, previous probability value is assigned. All the other groups, including ψ_0 and ψ_{K-1}, will have 0% probability after this stage. Lastly, histogram is scanned in reversed order to detect the groups whose probabilities exceed 100% when summed with the adjacent ones and their probabilities are updated to be 100%. The groups which don't satisfy this condition are directly assigned to 0% and dismissed from being a candidate threshold in our algorithm. Simply, the valleys corresponding to 100% probabilities are counted and that many thresholds are chosen as *candidate thresholds* T_{cdt} by the succeeding TSMO algorithm.

Otsu and its successor TSMO are both searching for the thresholds that either minimize within-class variance or maximize between-class variance, second is used and presented in this work. In a reconstruction problem, we have projections available; hence we also want to choose the thresholds from which minimize the projection error, which is used as the fidelity term in the unconstrained TvMin problem, given in Eq. 4.18. So the chosen threshold values should also satisfy the projection measurements. After the valley estimation and TSMO procedure, the candidate thresholds are obtained. These thresholds construct the search space for the cost function, given in Eq. 4.18, of the proposed method.

$$\tau_l^* = \underset{\tau \in T_{cdt}}{\operatorname{argmin}} \{ \sum_j \|D(x)_j\| + \frac{1}{2}\|b - Ax\|_2^2 \} \qquad \textbf{(4.18)}$$

where $D(x)_j$ is the discrete gradient of the image, $\|.\|$ denotes the $\ell_1 - norm$ and K is the number of candidate thresholds T_{cdt}.

Furthermore, to prevent high fluctuations caused by the segmentation step, a control operation is carried out after each threshold selection procedure. This operation

checks the difference between the current cost, given in Eq. 4.18, obtained by using the selected threshold and the previous cost and if this difference is greater than a predefined penalty parameter, the algorithm keeps using the previous threshold value instead of the selection. So, this operation might be defined as follows:

$$\tau^{(k)} = \begin{cases} \tau^{*}, & \Delta cost < \varepsilon_{penalty} \\ \tau^{(k-1)}, & otherwise \end{cases} \tag{4.19}$$

where Δ is used to denote the difference between current and previous costs, ε denotes the penalty parameter and τ^{*} is the selected optimum threshold value.

To demonstrate the effect of the proposed threshold selection procedure, two DART algorithms, one with Otsu's segmentation and another with the proposed segmentation are compared, and the results are shown in Fig. 4.4.

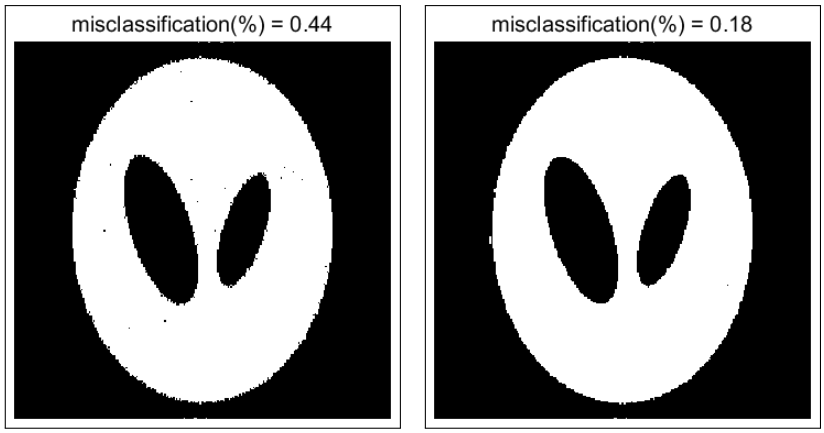

(a) Otsu, $r = 3$ (b) proposed, $r = 3$

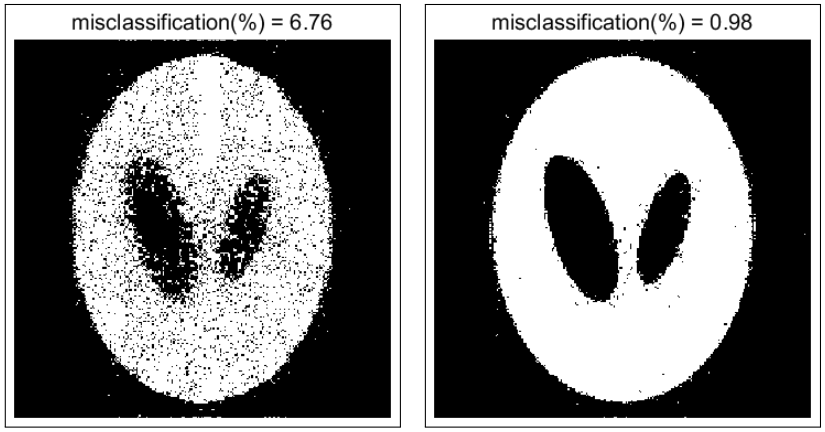

(c) Otsu, $r = 1$ (d) proposed, $r = 1$

Figure 4.4: A comparison between the reconstructions obtained by using Otsu and by the proposed threshold selection procedure (r is the Gaussian filter radius.)

Finally, the pseudo code and the flowchart of the proposed algorithm are given in Fig. 4.5 and Fig. 4.6, respectively.

Algorith 2 (TvMin+DART)

$x^{(0)} \longleftarrow TVAL3(x := 0, A, b), \quad k := 0$

while (*stop criterion is not met*) **do**

begin

Compute the histogram H^k

Estimate the number of valleys $L-1 \longleftarrow VE(H^k)$

Find K candidate thresholds $T_{cdt} \longleftarrow TSMO(H^k, L-1)$

Select threshold τ_l^* which makes Eq. 4.18 minimum

Segment image: $s^k \longleftarrow S(x^k, \tau^k)$

Subdivide s^k into free pixels $U^k \subset x^k$ and fixed $F^k = x^k \setminus U^k$

Extend U^k with the pixels in F^k with probability $1-p$

Compute the residual sinogram $r^k \longleftarrow b - Af^k$

Update the image of free pixels $u^k \longleftarrow ARM(u^k, A^k, r^k)$

Smooth u^k and obtain $x^{k+1} \longleftarrow f^k + u^k$

end

Figure 4.5: The pseudo code of the proposed TvMin+DART algorithm

The DART algorithm requires prior knowledge about the gray levels of the image. However, the gray levels might not be known (or they might erroneously be known) and that is why a requirement of automatic gray level (from now *label*) estimation is revealed. Finally, the proposed algorithm is extended to estimate gray levels to be applied in case of the exact labels are not known, in advance. The projection error is defined as follows:

$$E(x) \quad = \quad \|b - b^{'}\| \quad = \quad \sum_{i}^{m} (b_i - b_i^{'})^2 \tag{4.20}$$

It can be rewritten as in Eq. 4.21 by substituting the forward projection of the labelled image $x_j \in \{\xi_1, \xi_2, .., \xi_L\}$ where ξ_l denotes the labels.

$$E(x) = \sum_{i}^{m} (b_i - \sum_{l=1}^{L} \xi_l Q_{il})^2 \quad where \quad Q_{il} = \sum_{j \in \Omega_l} a_{ij} \tag{4.21}$$

Since Eq. 4.21 is differentiable to ξ_l, by taking the derivative of it with respect to the ξ_l to find the labels which minimize the error, one comes up with the following solution:

$$\begin{aligned}
\frac{\partial E}{\partial \xi_l} &= \frac{\partial}{\partial \xi_l}\{\sum_{i=1}^{m}(b_i - \sum_{l=1}^{L}\xi_l Q_{il})^2\} \\
&= \frac{\partial}{\partial \xi_t}\{\sum_{i=1}^{m}(b_i - (\sum_{\substack{l=1 \\ l\neq t}}^{L}\xi_l Q_{il} + Q_{it}\xi_t))^2\} \\
&= -2\{\sum_{i=1}^{m}(b_i Q_{it} - \sum_{\substack{l=1 \\ l\neq t}}^{L} Q_{il}Q_{it}\xi_l - Q_{it}^2\xi_t)\} \\
&= -2\sum_{i=1}^{m} Q_{it}(b_i - \sum_{\substack{l=1 \\ l\neq t}}^{L} Q_{il}\xi_l) + 2\xi_t\sum_{i=1}^{m} Q_{it}^2
\end{aligned} \tag{4.22}$$

where $t = 1,..,n$. Therefore, the gray levels can easily be estimated by using the following equation:

$$\xi_t = \frac{\sum_{i=1}^{m} Q_{it}(b_i - \sum_{\substack{l=1 \\ l\neq t}}^{L} Q_{il}\xi_l)}{\sum_{i=1}^{m} Q_{it}^2}. \tag{4.23}$$

Once Eq. 4.23 is computed, the previous gray level set is updated with the new labels and this procedure is repeated for each iteration, after the thresholds are determined and the image is segmented.

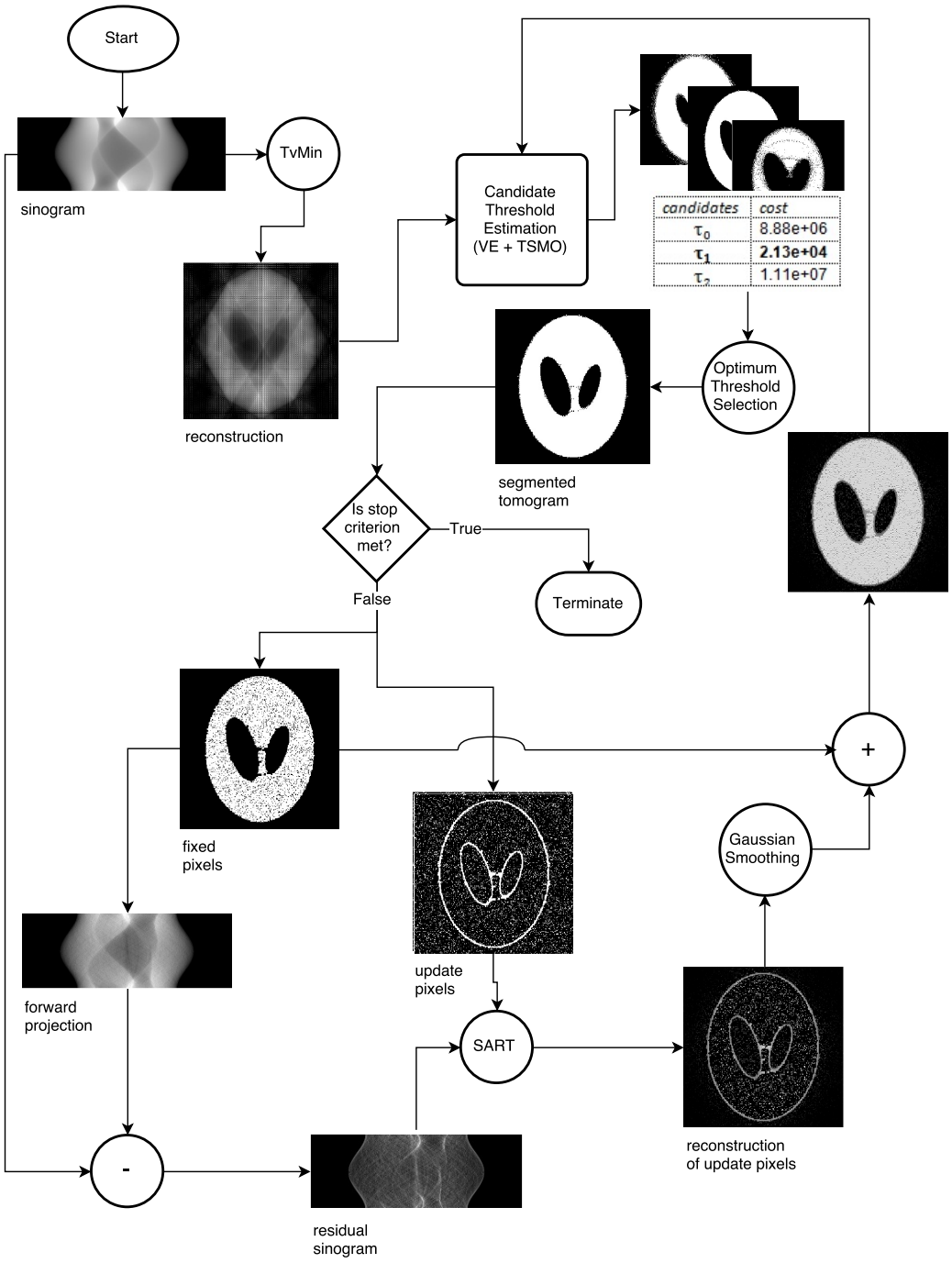

Figure 4.6: A schematic overview of the proposed algorithm

5. SIMULATION EXPERIMENTS

In this chapter, the results obtained via the proposed algorithm, named as TvMin+DART for simplicity while referring, is presented and TvMin+DART is compared to the original DART, plus segmented FBP. The DART algorithm is implemented as described in [5] and FBP is performed using inverse Radon transform (*iradon*) function in MATLAB with linear interpolation and Ram-Lak filter and segmented using Otsu's thresholding scheme. TvMin+DART algorithm is also implemented in MATLAB environment. AIR Tools package [39] is exploited for the simulation of the parallel beam geometry and the required ARM algorithm. To solve the TvMin problem, TVAL3 MATLAB solver [36] [33] is used.

To start with introducing the performance evaluation metrics, misclassification percentage, given in Eq. 5.1, root means squared error (RMSE), given in Eq. 5.2 and root means squared projection error (RMSPE), given in Eq. 5.3 are used where x' denotes the reconstructed image, b' is the forward projection of x'.

$$misclassification(\%) = \frac{100}{n}\sum_{j=1}^{n}(1-\delta(x,x')) \tag{5.1}$$

where δ is the Dirac delta function known as: $\delta(x-x') = \begin{cases} 1, & x = x' \\ 0, & x \neq x' \end{cases}$

$$RMSE = \left(\frac{\sum_{j=1}^{n}(x_j - x'_j)^2}{n}\right)^{1/2} \tag{5.2}$$

where n is the total number of pixels.

$$RMSPE = \left(\frac{E(x)}{m}\right)^{1/2} \tag{5.3}$$

where m is the number of the projection measurements and $E(x)$ is the projection error defined as $E(x) = \|b-b'\|_2 = \sum_{i=1}^{m}(b_i - b'_i)^2$.

The test images used in the simulation experiments are given in Fig. 5.1. They differ in size; while Phantom-1 is 128 by 128, Phantom-2, Phantom-4 and Phantom-5 are all

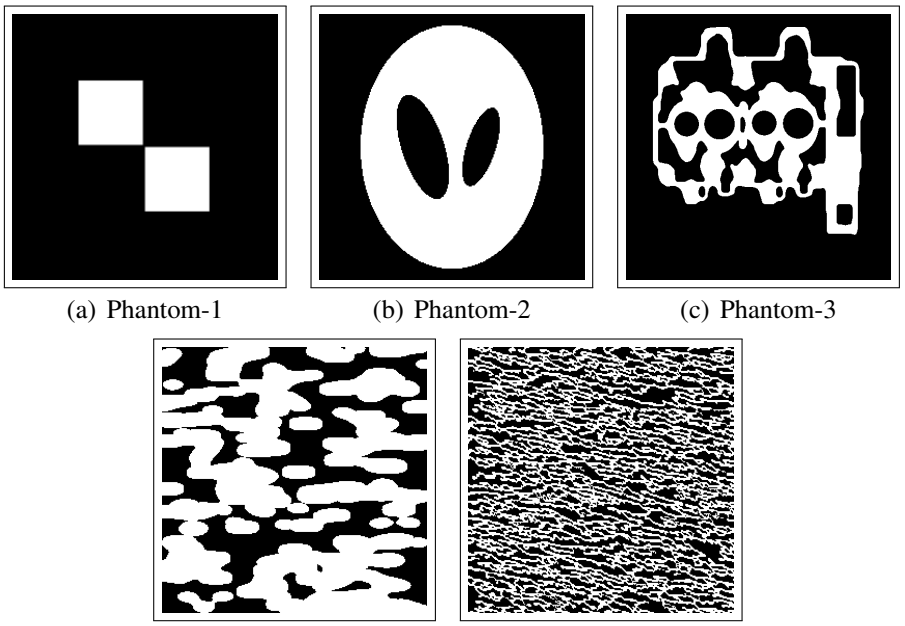

(a) Phantom-1 (b) Phantom-2 (c) Phantom-3

(d) Phantom-4 (e) Phantom-5

Figure 5.1: Phantom images used for the experiments

256 by 256 and Phatom-3 is 512 by 512 pixels. Phantom-2 is a binarized version of well-known Sheep-Logan phantom, Phantom-3 is same with one of the phantoms used in the paper [5], in which the original DART is proposed. Phantom-4 and Phantom-5 are both taken from the phantom gallery which comes with AIR Tools package [39].

There are several parameters to be used. The number of variables, so the total number of pixels, depends on the phantom sizes which are stated above. The ARM, which will be used for subsequent updates of both the DART and the TvMin+DART, is chosen as the SART algorithm. Hence, the algorithm used to obtain the initial estimate will also be the SART algorithm for the DART. Unconstrained TvMin model (with the fidelity term) is used, to choose an initial estimate which minimizes both the projection error and the ℓ_1 norm of the discrete gradient, but the non-negativity constraint is also considered. For the sake of practicability, some parameters, such as the relaxation parameter (λ) of SART as 0.8 (as suggested in [39]), the radius of the Gaussian smoothing filter as 3 (default) and the fix probability (p) as 0.85 (as suggested in [5]). The randomized procedure is applied both the DART and the TvMin+DART algorithms simultaneously, meaning that the update pixels, which are selected with fix probability, are determined once and used for both algorithms. Also, the number of the initial estimation iterations (t_0) for the TvMin and the SART are both fixed to 3, like the subsequent SART iterations (t) which are also set to 3. For all experiments, only

the binary images are considered. The algorithm can be extended to be used for the images with multiple gray levels, in a straightforward manner. Except the last section, in all experiments, the exact gray levels $\{0,1\}$, in our case) are assumed to be known and used. The remaining parameters such as, the number of the projections (s), the angular range (θ), the number of the iterations (k) and the noise level (η), are all the parameters that are considered separately and used while comparing the performances of the algorithms.

5.1 Limited Number of Projections

In this section, varying number of equidistant projections, which are sampled between $[0,\pi)$, are taken into consideration. FBP, the original DART and the proposed TvMin+DART are compared in terms of the reconstruction quality, which is determined by using the metric *misclassification(%)*, as a function of the number of the projections. While the reconstruction results of the TvMin+DART algorithm are presented in Fig. 5.5 for several number of projections, the reconstructed images obtained from the FBP and the DART are shown in Fig. 5.6, together with the results of the proposed method, using a certain number of projections for each phantom. For all simulations carried out in this section, $k = 200$ number of iterations are used.

In Fig. 5.2 and Fig. 5.3, the misclassification percent of the reconstruction obtained using the proposed algorithm is more or less lower than the FBP and the DART. While number of projections are being increased, obvious improvements are observed, it is also seen that the FBP algorithm isn't good at reconstructing satisfying results in both Fig. 5.2 and Fig. 5.3. However, an unexpected result is observed in Fig. 5.4 that the FBP algorithm yields better reconstructions than the iterative methods even for the small number of projections. That is caused due to the morphology of Phantom-5. As it is inferred from the results, iterative methods are tend to compute better reconstructions for more rigid, symmetric and homogeneous patterns than the bulk ones as in Fig. 5.1 (e). Furthermore, as it is understood from the results, to obtain a satisfying reconstruction, different number of projections are used for different phantoms. For instance, while $s = 8$ seems to be enough for Phantom-2, the reconstruction of Phantom-3 is poor when $s = 8$ (see Fig. 5.5). So, this knowledge is exploited for the succeeding simulation experiments.

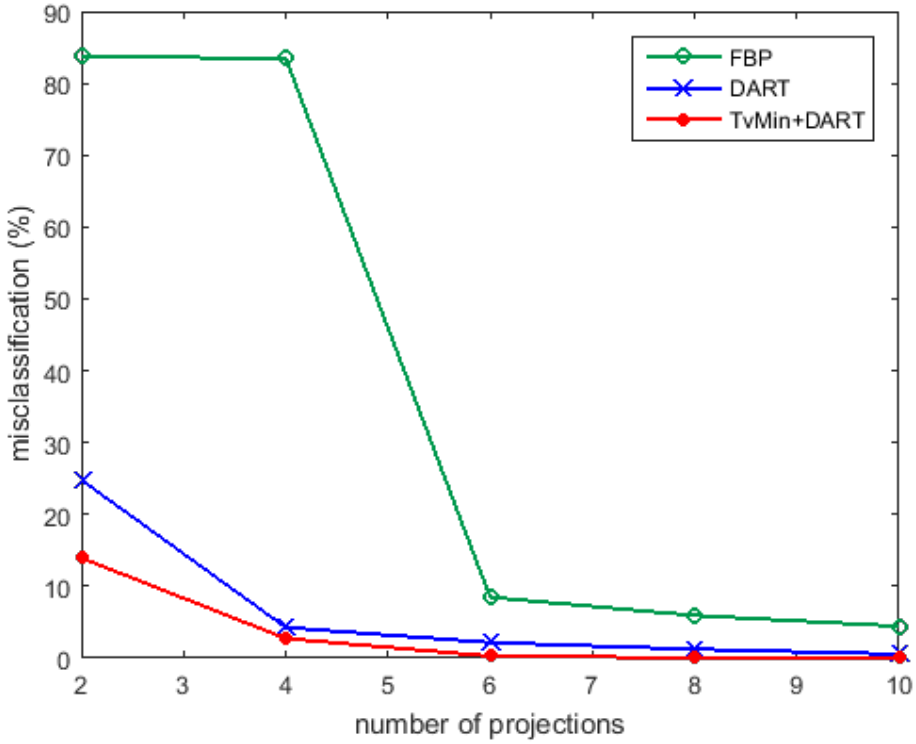

(a) Phantom-1

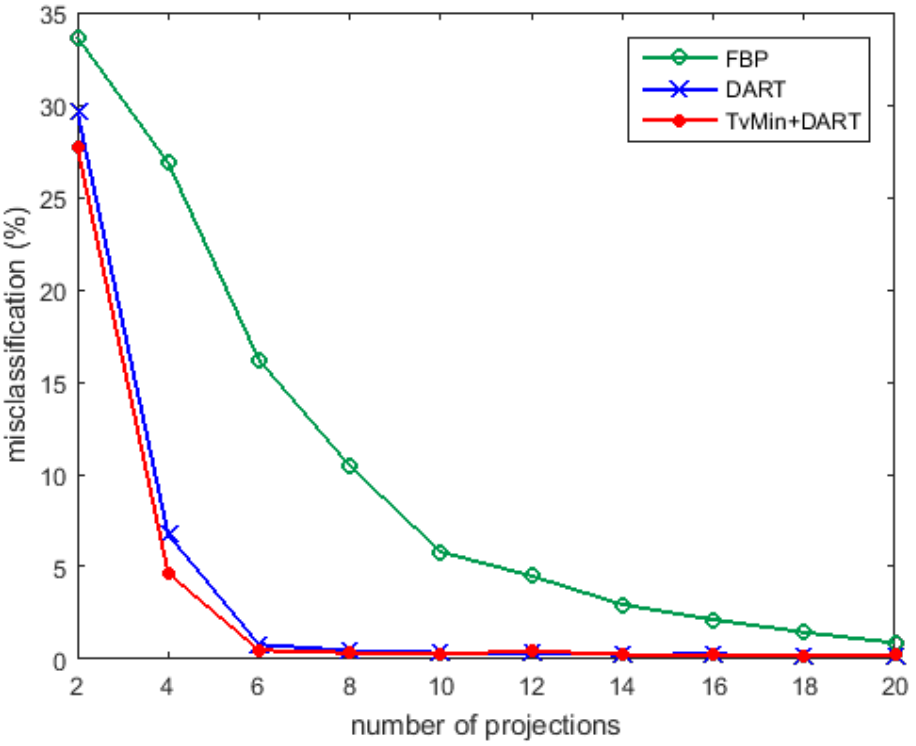

(b) Phantom-2

Figure 5.2: The misclassification percent with respect to the number of projections for Phantom-1 and Phantom-2

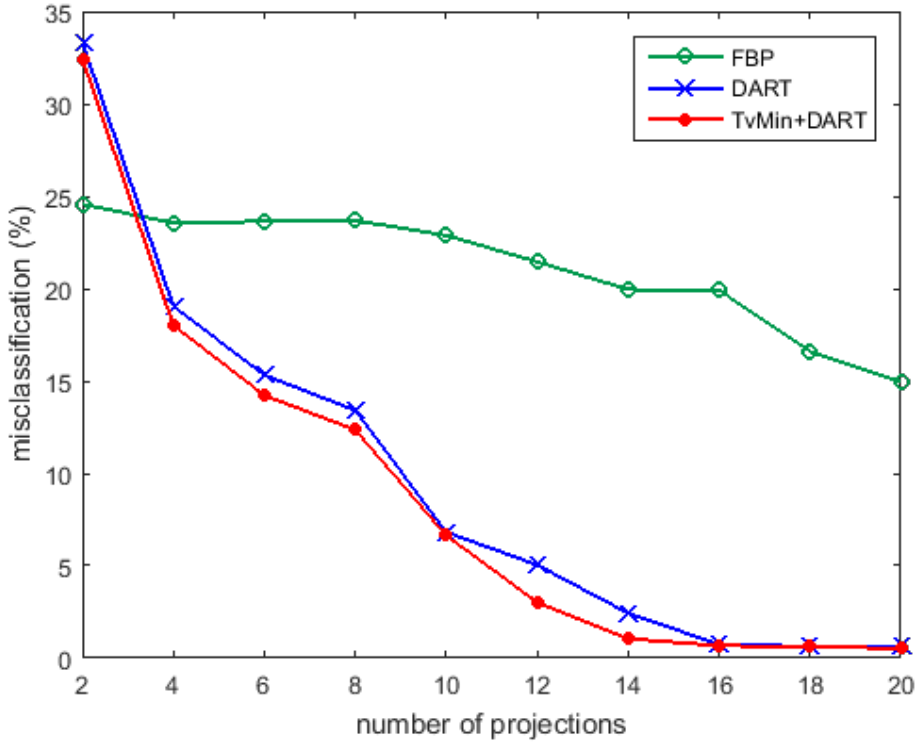

(a) Phantom-3

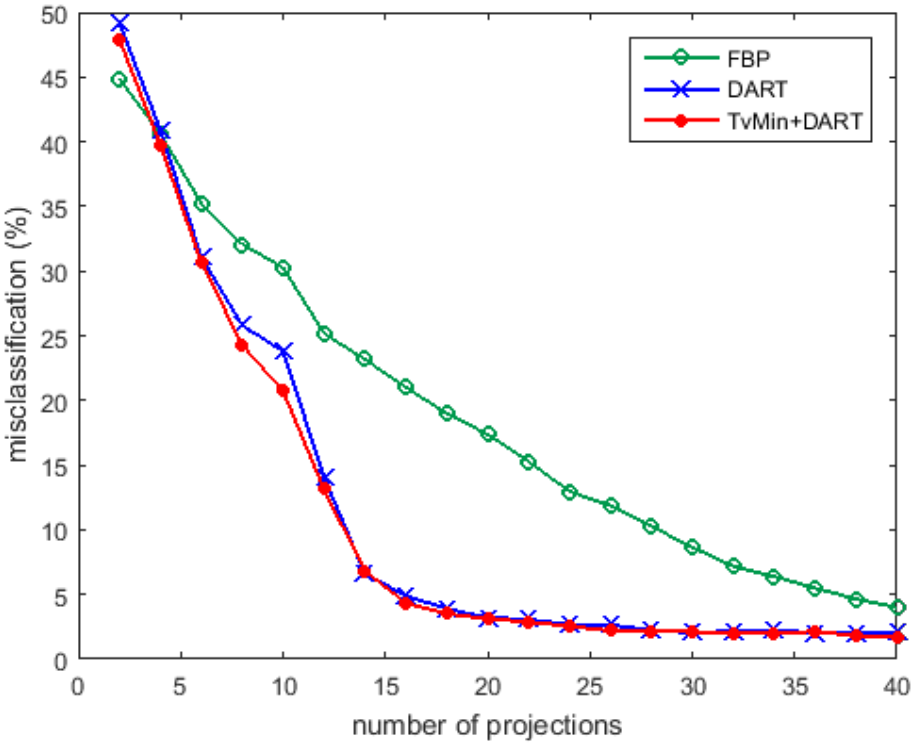

(b) Phantom-4

Figure 5.3: The misclassification percent with respect to the number of projections for Phantom-3 and Phantom-4

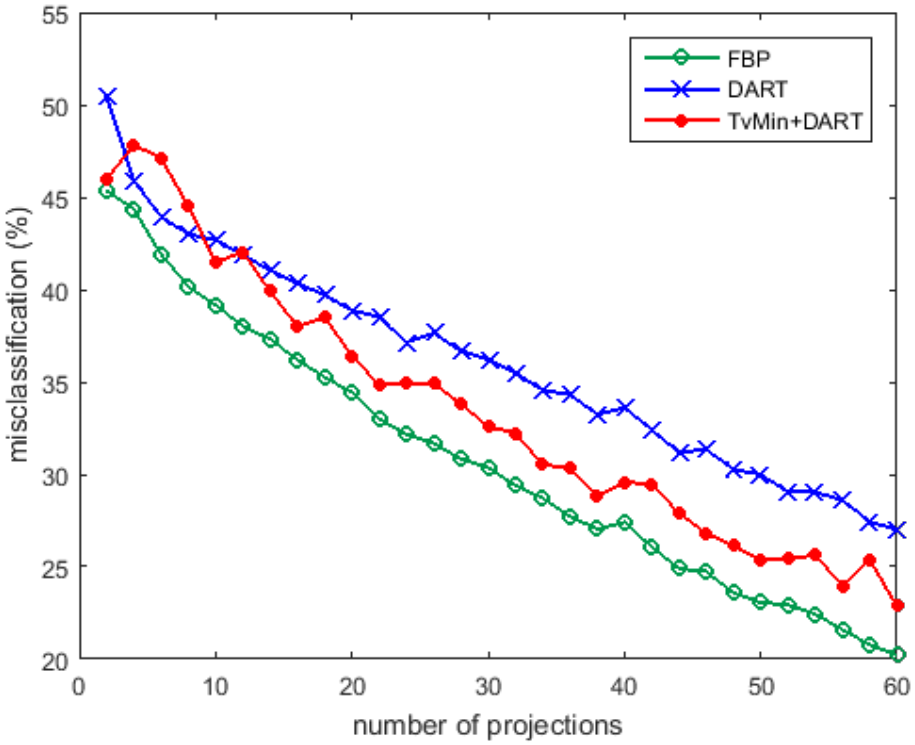

(a) Phantom-5

Figure 5.4: The misclassification percent with respect to the number of projections for Phantom-5

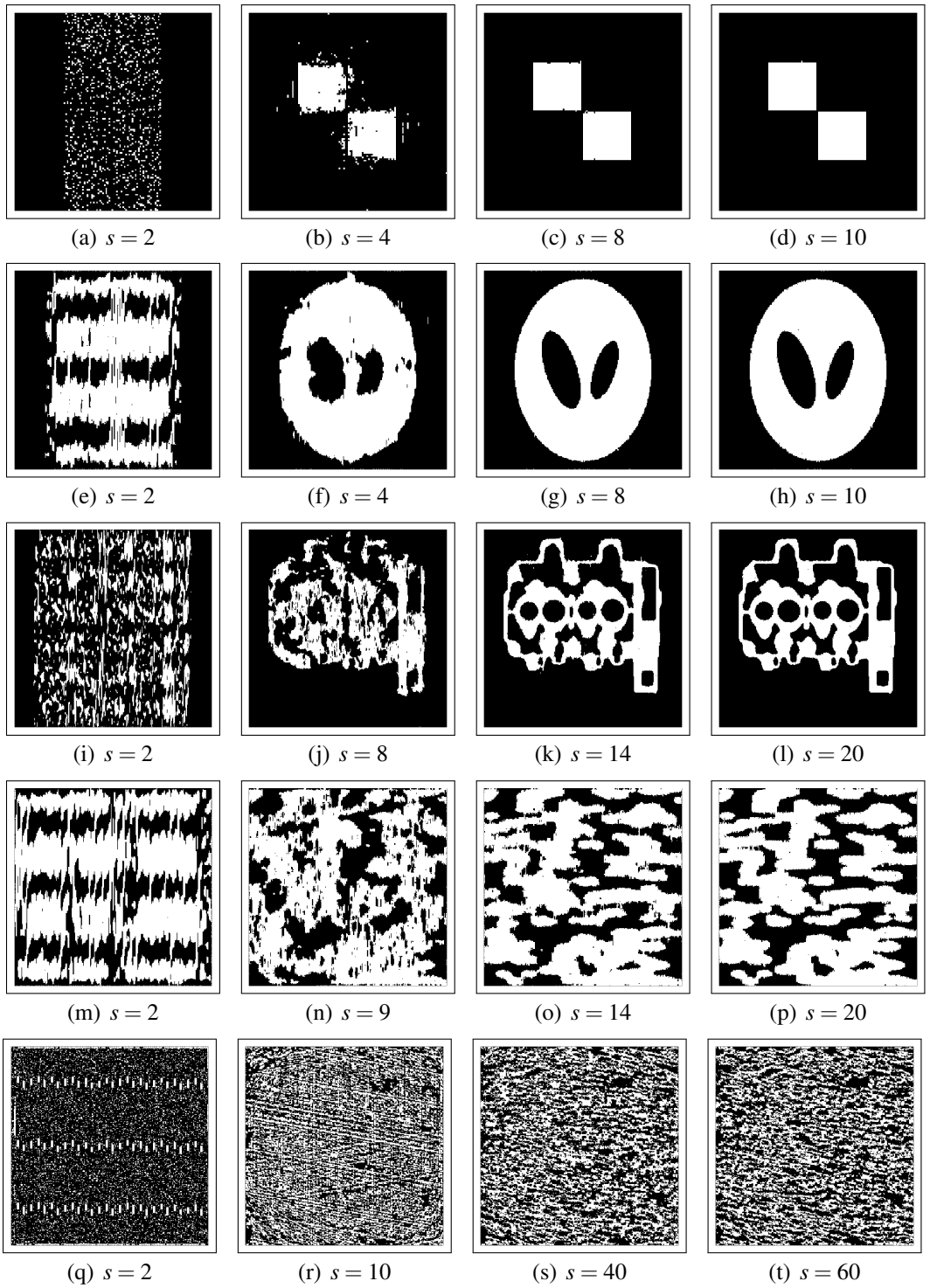

(a) $s = 2$ (b) $s = 4$ (c) $s = 8$ (d) $s = 10$

(e) $s = 2$ (f) $s = 4$ (g) $s = 8$ (h) $s = 10$

(i) $s = 2$ (j) $s = 8$ (k) $s = 14$ (l) $s = 20$

(m) $s = 2$ (n) $s = 9$ (o) $s = 14$ (p) $s = 20$

(q) $s = 2$ (r) $s = 10$ (s) $s = 40$ (t) $s = 60$

Figure 5.5: TvMin+DART reconstruction of the phantoms from Phantom-1 to Phantom-5, from the top row to bottom, using number of projections s.

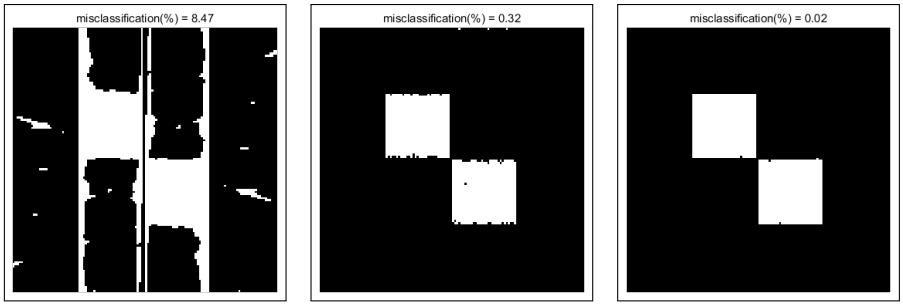

(a) FBP, $s = 6$ (b) DART, $s = 6$ (c) TvMin+DART, $s = 6$

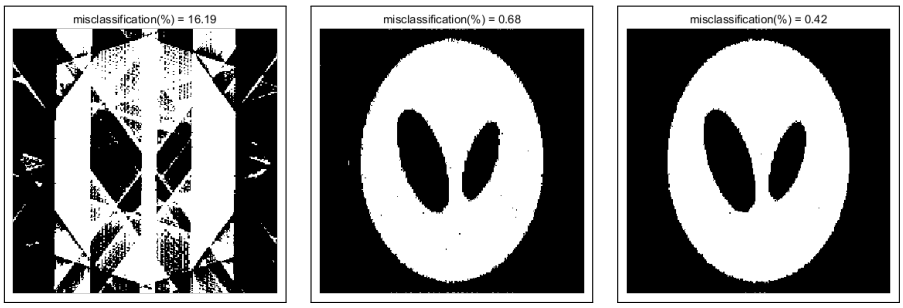

(d) FBP, $s = 6$ (e) DART, $s = 6$ (f) TvMin+DART, $s = 6$

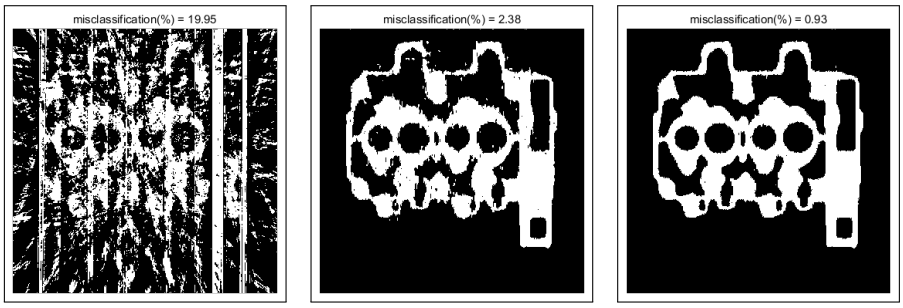

(g) FBP, $s = 14$ (h) DART, $s = 14$ (i) TvMin+DART, $s = 14$

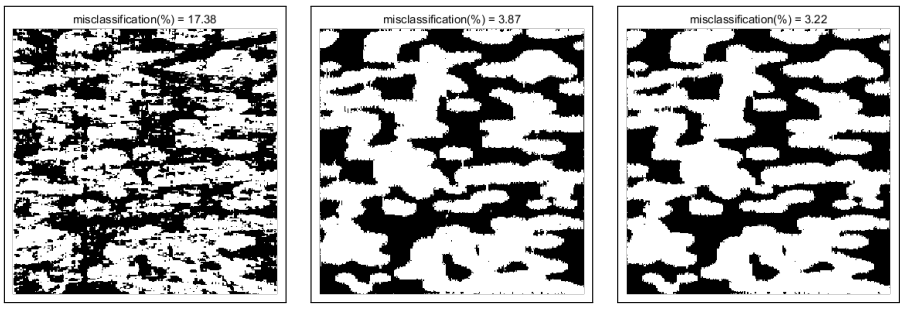

(j) FBP, $s = 20$ (k) DART, $s = 20$ (l) TvMin+DART, $s = 20$

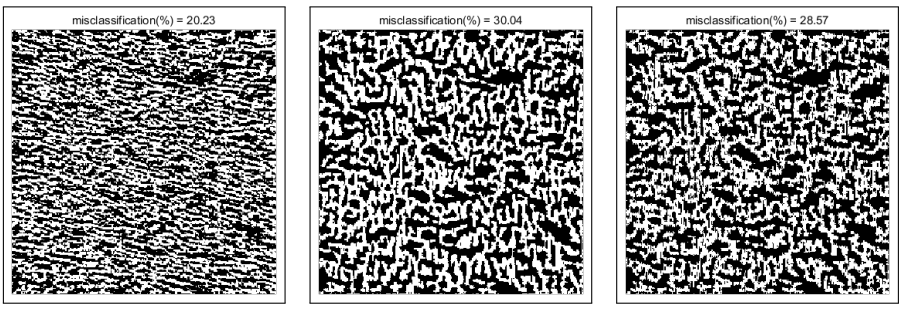

(m) FBP, $s = 60$ (n) DART, $s = 60$ (o) TvMin+DART, $s = 60$

Figure 5.6: A comparison of FBP, DART and TvMin+DART reconstructions of the phantoms from Phantom-1 to Phantom-5, from the top row to bottom, using number of projections s.

5.2 Limited View Problem

In this section, the full range is narrowed down from $[0, \pi)$ to $[4\pi/9, 5\pi/9)$, gradually and sampled the projections at 1 degree intervals for each range, to simulate limited view. The reconstruction accuracy of the FBP, the original DART and the proposed TvMin+DART are compared using *misclassification(%)* percentage as a function of the angular range. The results are presented graphically in Fig. 5.7, Fig. 5.8 and Fig. 5.9 and the reconstructed images are shown in Fig. 5.10 and Fig. 5.11. All simulations are performed by using $k = 200$ number of iterations.

In Fig. 5.7 (a), almost exact solution is reached by the TvMin+DART algorithm for 120-degree range, while it is the case for the FBP and the DART, when the range is 180. On the other hand, the DART algorithm yields better reconstructions of Phantom-2 for the narrower ranges, between 20 and 80; however the almost exact result is obtained by TvMin+DART algorithm for the 120-degree angular range, as it is shown in Fig. 5.7 (b). The results of the DART and the TvMin+DART for Phantom-3 and Phantom-4 are shown in Fig. 5.8 (a) and (b), respectively and the misclassification percentages are almost same for each angular ranges and both algorithms are reaching the accurate solution when the range becomes 160 for Phantom-3. In Fig. 5.8 (b), nevertheless, the accurate solution cannot be computed by both iterative algorithms, even for full range. The FBP, on the contrary, results with the accurate reconstruction of Phantom-3, for the case of full range; although its failure for the former phantoms and the narrower ranges. For Phantom-5, the same situation with the limited number of projections experiment is encountered and the FBP yield much better results for each angular ranges, as it can be seen in Fig. 5.9. Finally, the increased range gradually improves the solution as it can be inferred from each experiment and for each algorithm.

In Fig. 5.10 and Fig. 5.11, the reconstructions obtained by TvMin+DART algorithm for various angular ranges and the reconstructions obtained by the FBP, the DART and the proposed algorithm for certain angular ranges are shown, respectively. As it is seen from the latter one, TvMin+DART results with slightly better reconstructions than the ones obtained by the DART algorithm, for Phantom 1 to 3.

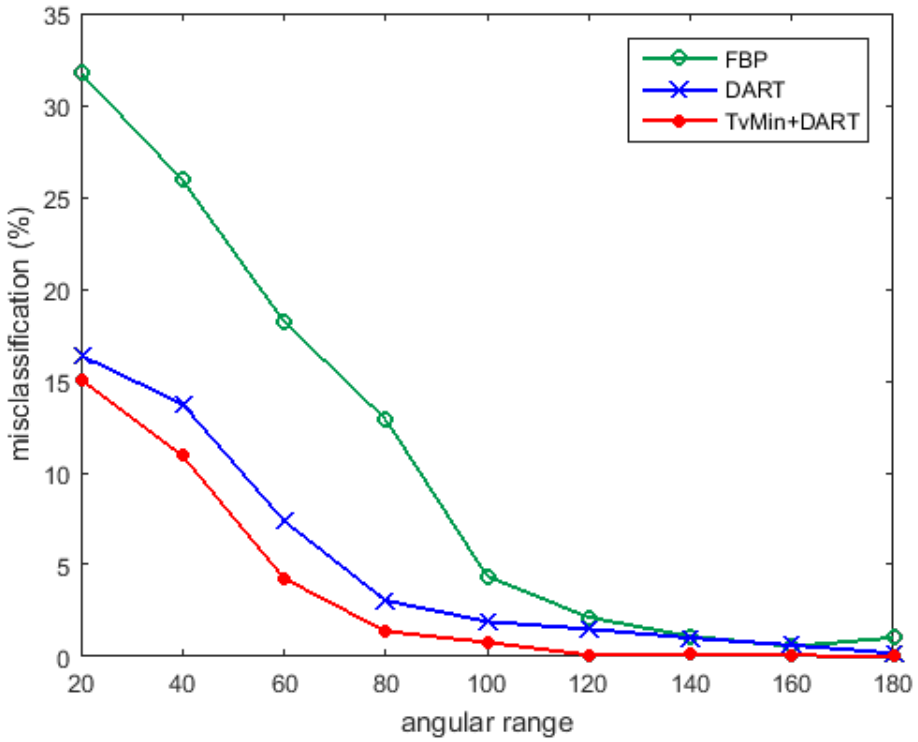

(a) Phantom-1

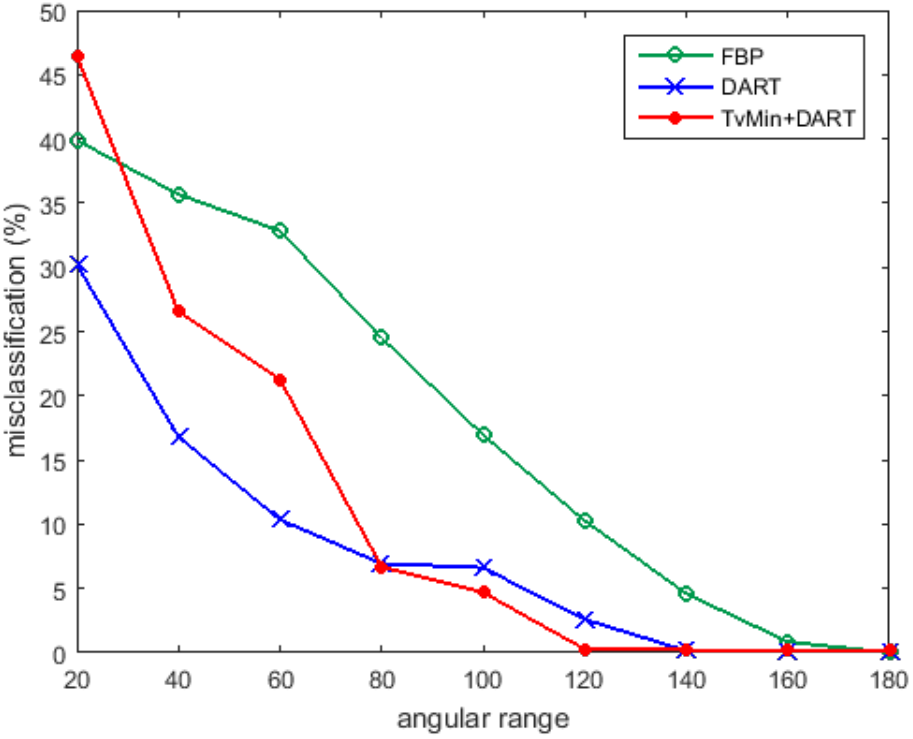

(b) Phantom-2

Figure 5.7: The misclassification percent with respect to the angular range for Phantom-1 and Phantom-2

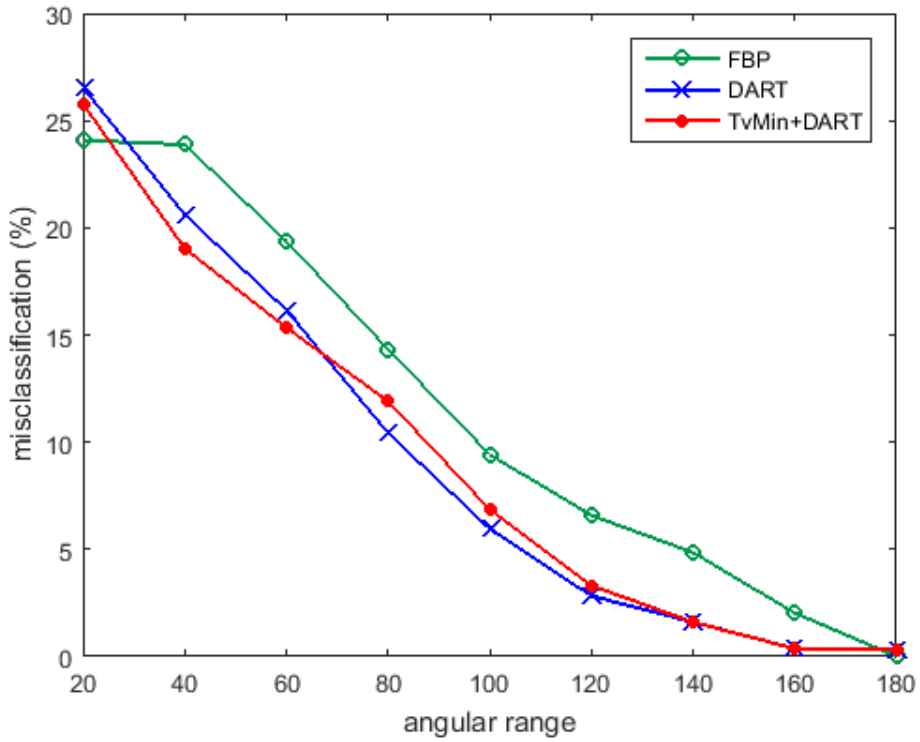

(a) Phantom-3

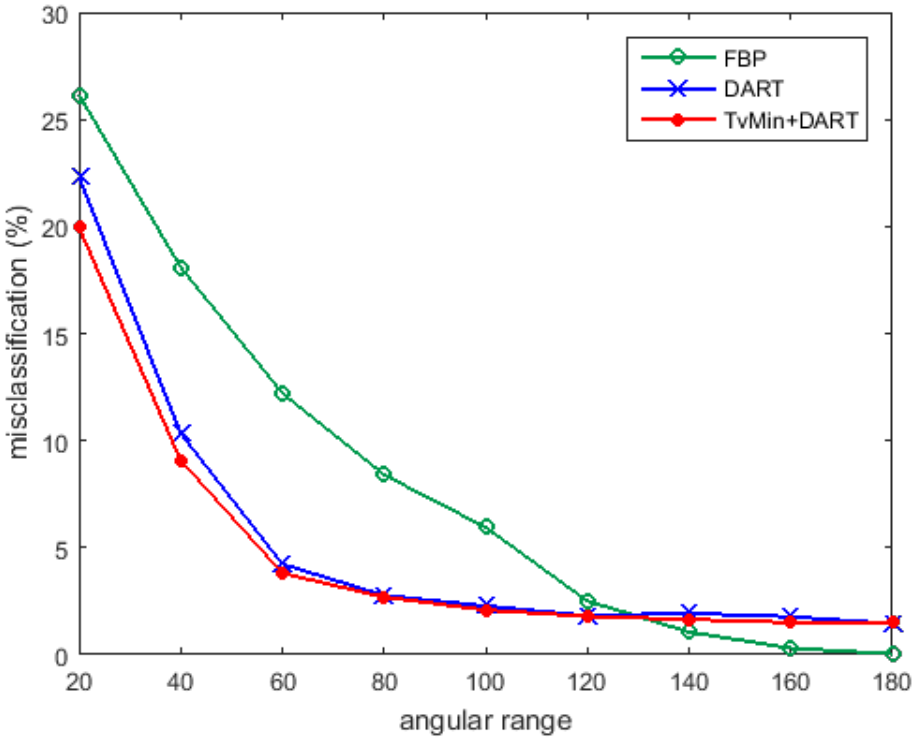

(b) Phantom-4

Figure 5.8: The misclassification percent with respect to the angular range for Phantom-3 and Phantom-4

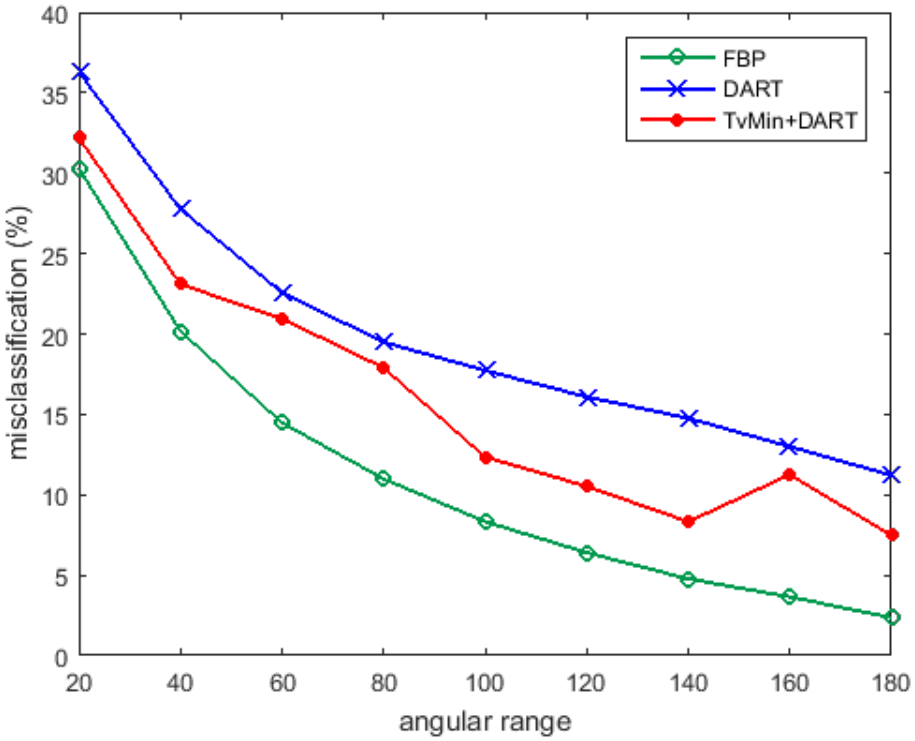

(a) Phantom-5

Figure 5.9: The misclassification percent with respect to the angular range for Phantom-5

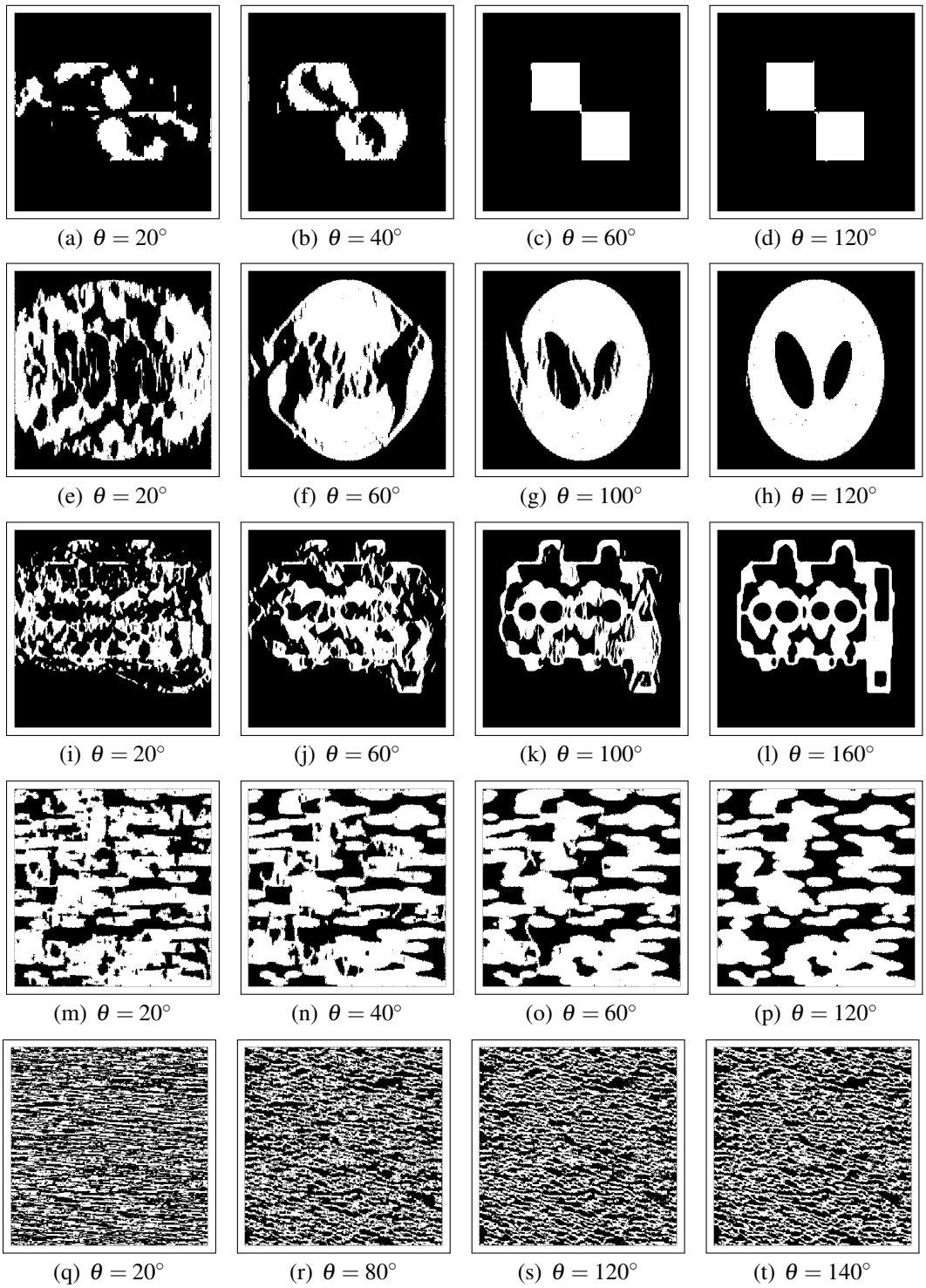

(a) $\theta = 20°$ (b) $\theta = 40°$ (c) $\theta = 60°$ (d) $\theta = 120°$

(e) $\theta = 20°$ (f) $\theta = 60°$ (g) $\theta = 100°$ (h) $\theta = 120°$

(i) $\theta = 20°$ (j) $\theta = 60°$ (k) $\theta = 100°$ (l) $\theta = 160°$

(m) $\theta = 20°$ (n) $\theta = 40°$ (o) $\theta = 60°$ (p) $\theta = 120°$

(q) $\theta = 20°$ (r) $\theta = 80°$ (s) $\theta = 120°$ (t) $\theta = 140°$

Figure 5.10: TvMin+DART reconstruction of the phantoms from Phantom-1 to Phantom-5, from the top row to bottom, using angular range θ.

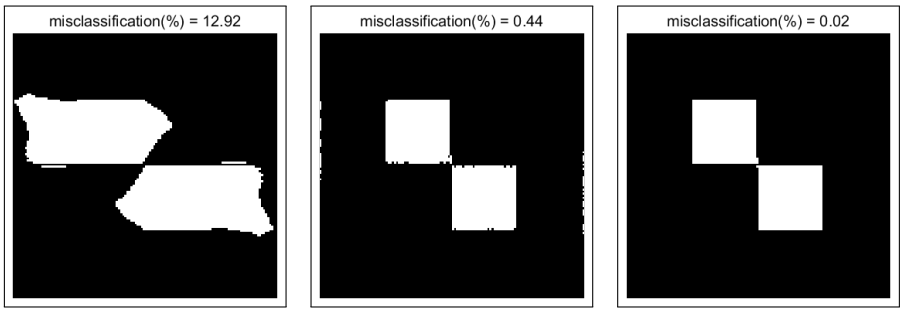

(a) FBP, $\theta = 80°$ (b) DART, $\theta = 80°$ (c) TvMin+DART, $\theta = 80°$

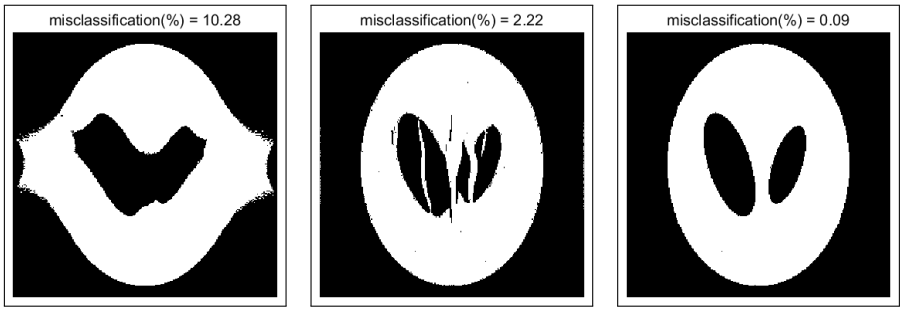

(d) FBP, $\theta = 120°$ (e) DART, $\theta = 120°$ (f) TvMin+DART,$\theta = 120°$

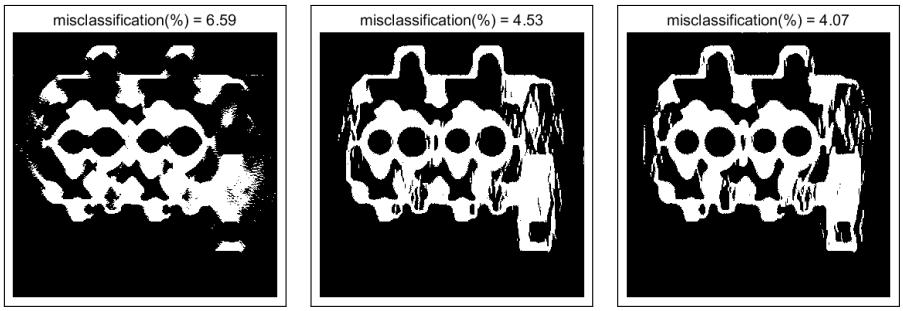

(g) FBP, $\theta = 120°$ (h) DART, $\theta = 120°$ (i) TvMin+DART,$\theta = 120°$

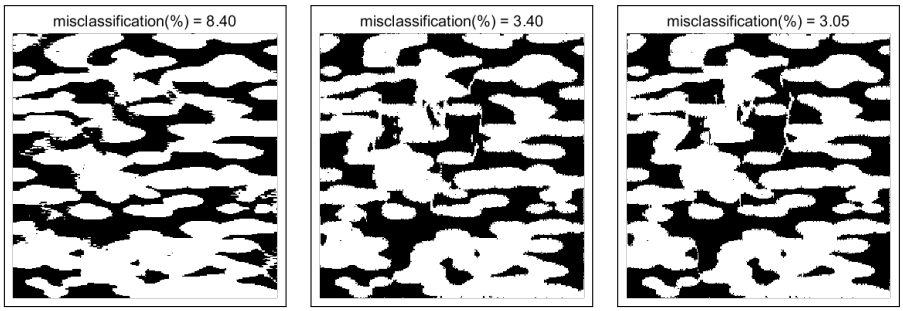

(j) FBP, $\theta = 80°$ (k) DART, $\theta = 80°$ (l) TvMin+DART, $\theta = 80°$

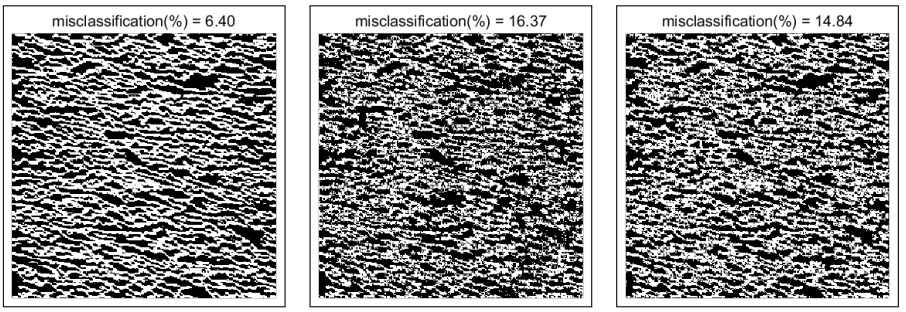

(m) FBP, $\theta = 120°$ (n) DART, $\theta = 120°$ (o) TvMin+DART,$\theta = 120°$

Figure 5.11: A comparison of FBP, DART and TvMin+DART reconstructions of the phantoms from Phantom-1 to Phantom-5, from the top row to bottom, using number of projections using angular range θ.

5.3 Noisy Projections

In the former sections, noise-free projection measurements were used. In this section, the robustness of the algorithms with respect to noise are compared. To simulate a noisy projection, the projection samples are polluted by adding a noise vector on them, as in Eq. 5.4.

$$\tilde{b} = b + \eta \|b\| \frac{e}{\|e\|} \tag{5.4}$$

where e is a random noise vector and $\tilde{b}$ denotes the noisy projection measurements.

In Fig. 5.13, Fig. 5.14 and Fig. 5.12, the misclassification percentage as a function of the noise level (η) is shown graphically. The noise levels $\eta \in \{0, 0.05, 0.1, 0.15, 0.2\}$ are used, where $\eta = 0.05$ is the most reasonable one. The number of the projections are restricted with the values s = 6, 8, 14, 40 and 60 for Phantom 1 to 5, respectively. The proposed method yields slightly better results when compared to the DART algorithm, for almost every phantoms (except $\eta = 0.05$ and $\eta = 0.1$ for Phantom-4, in Fig. 5.14 (b)). As it can easily be seen, the FBP is highly sensitive to noise.

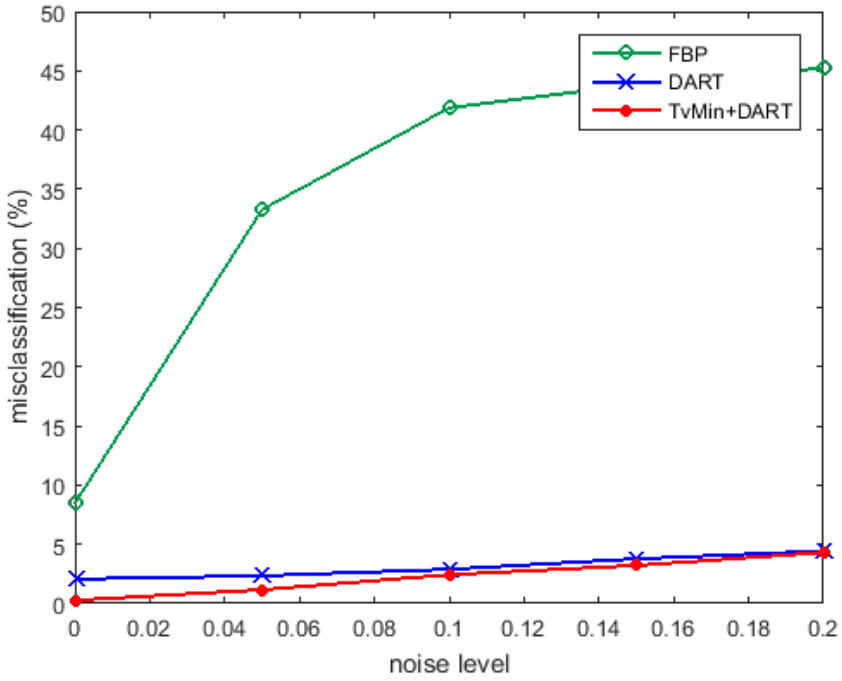

(a) Phantom-1, $s = 6$

Figure 5.12: The misclassification percent with respect to the noise level for Phantom-5

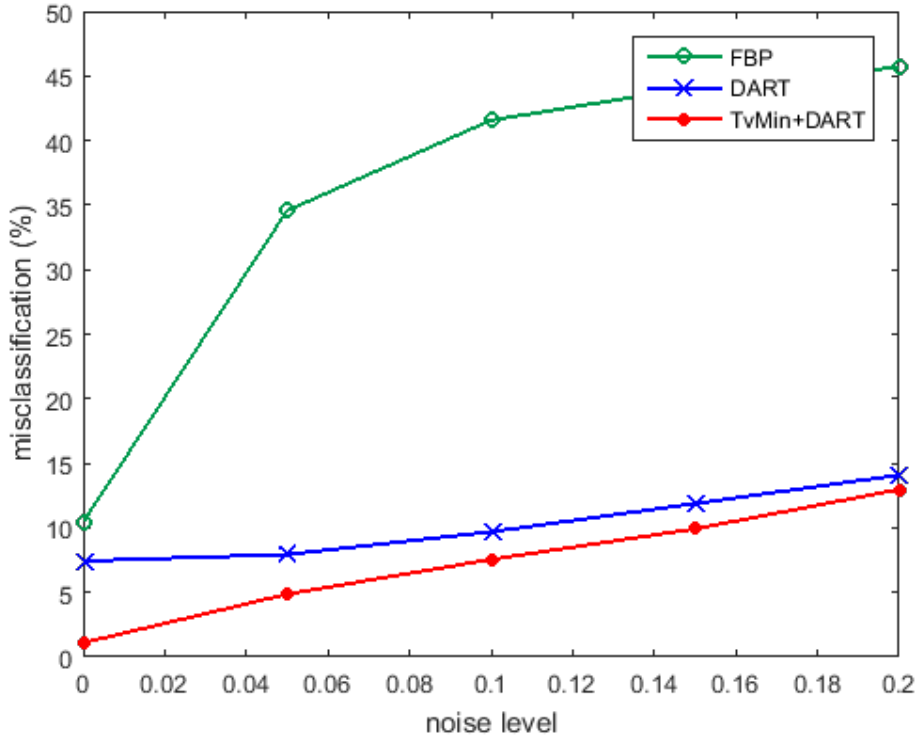

(a) Phantom-2, $s = 8$

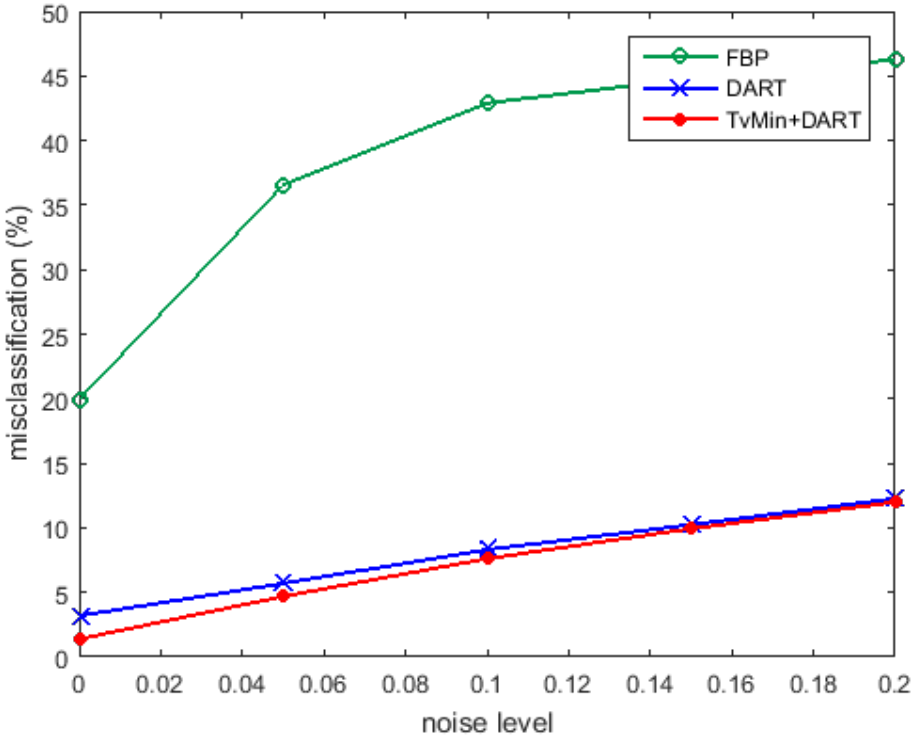

(b) Phantom-3, $s = 14$

Figure 5.13: The misclassification percent with respect to the noise level for Phantom-1 and Phantom-2

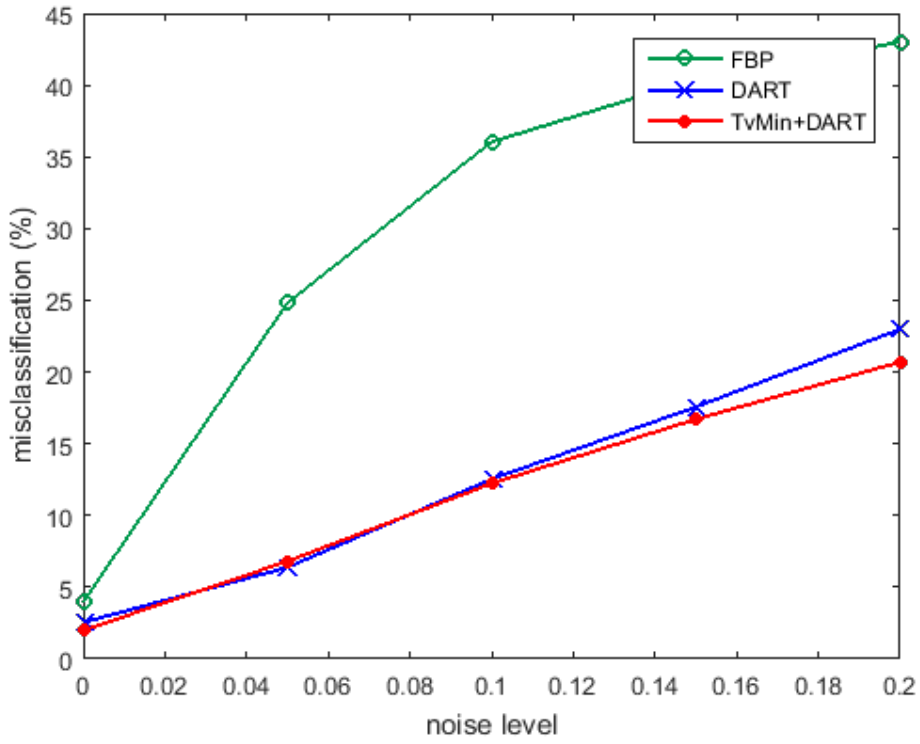

(a) Phantom-4, $s = 40$

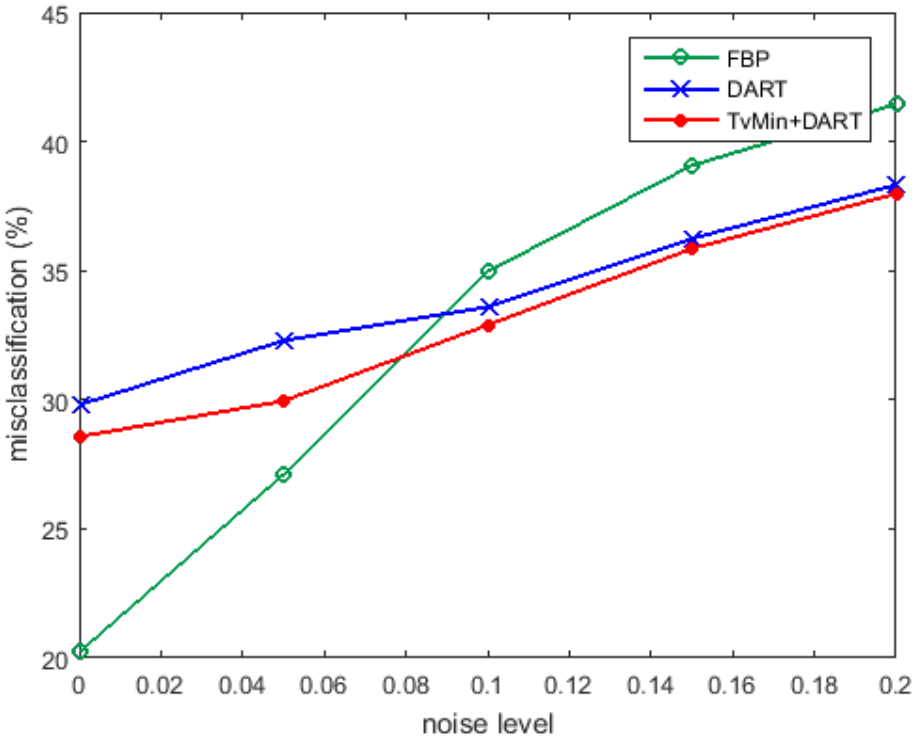

(b) Phantom-5, $s = 60$

Figure 5.14: The misclassification percent with respect to the noise level for Phantom-3 and Phantom-4

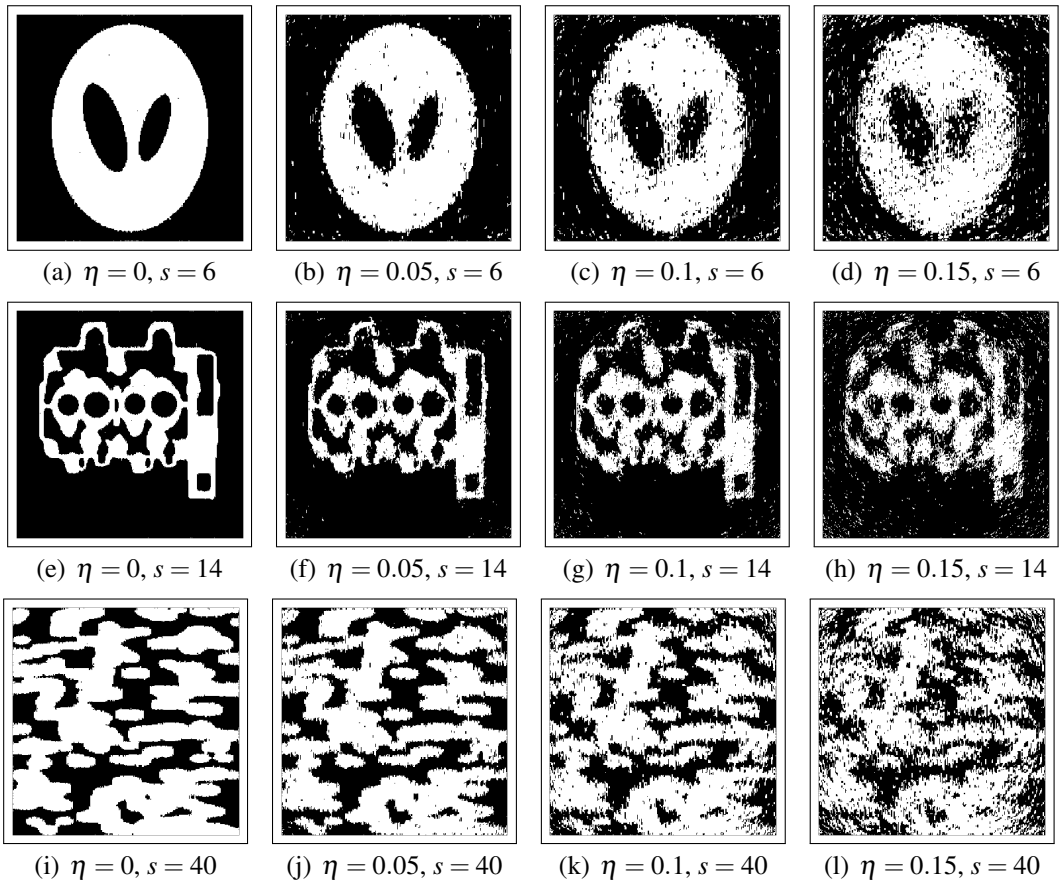

(a) $\eta = 0$, $s = 6$ (b) $\eta = 0.05$, $s = 6$ (c) $\eta = 0.1$, $s = 6$ (d) $\eta = 0.15$, $s = 6$

(e) $\eta = 0$, $s = 14$ (f) $\eta = 0.05$, $s = 14$ (g) $\eta = 0.1$, $s = 14$ (h) $\eta = 0.15$, $s = 14$

(i) $\eta = 0$, $s = 40$ (j) $\eta = 0.05$, $s = 40$ (k) $\eta = 0.1$, $s = 40$ (l) $\eta = 0.15$, $s = 40$

Figure 5.15: TvMin+DART reconstruction from noisy projections with noise level η and the number of projections s.

5.4 An Experiment on Spatial Resolution

In this short section, the accuracies of the subjected algorithms are compared in terms of the misclassification as a function of cycles/pixels. Cycles are represented by the line pairs, shown in Fig. 5.16 with increasing line widths from 1 pixel to 5 pixels. So, the cycles/pixel ratio is decreasing from 0.5 to 0.2, when the widths are increasing, from Fig. 5.16 (a) to Fig. 5.16 (e). Since the images are discrete and have only two gray values, the misclassification metric is found adequate for this study but one can use different spatial resolution metrics, such as modulation transfer function (MTF), and measure the spatial resolutions of the algorithms, either in spatial or in frequency domain. In Fig. 5.17, the proposed method couldn't result with a better reconstruction for the image with highest frequency. The FBP has given more accurate results than the iterative ones, for the each pattern used in this experiment. The number of projections is set to s= 20, for the reconstruction of each line pattern.

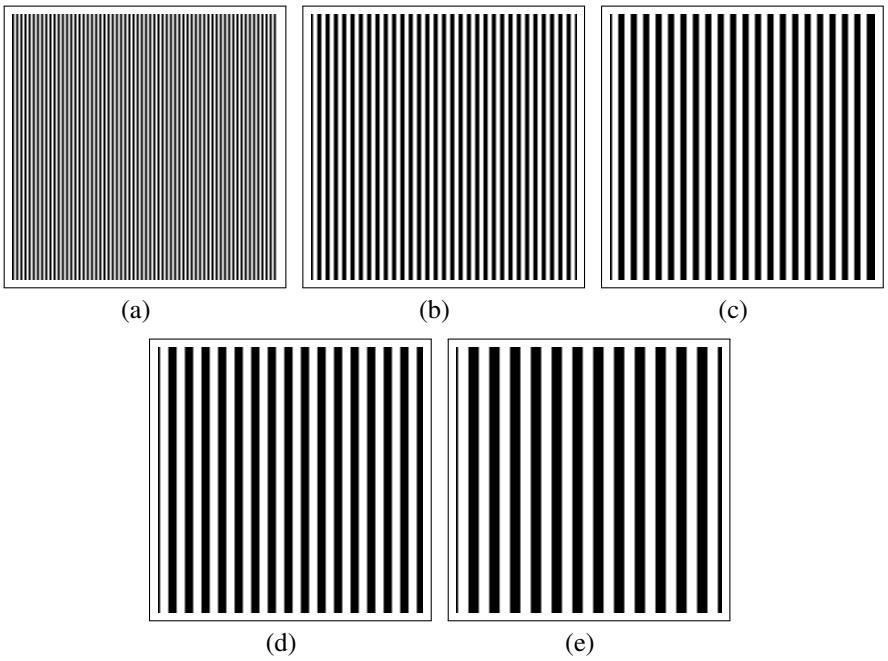

Figure 5.16: Line pair patterns, used to test spatial resolution.

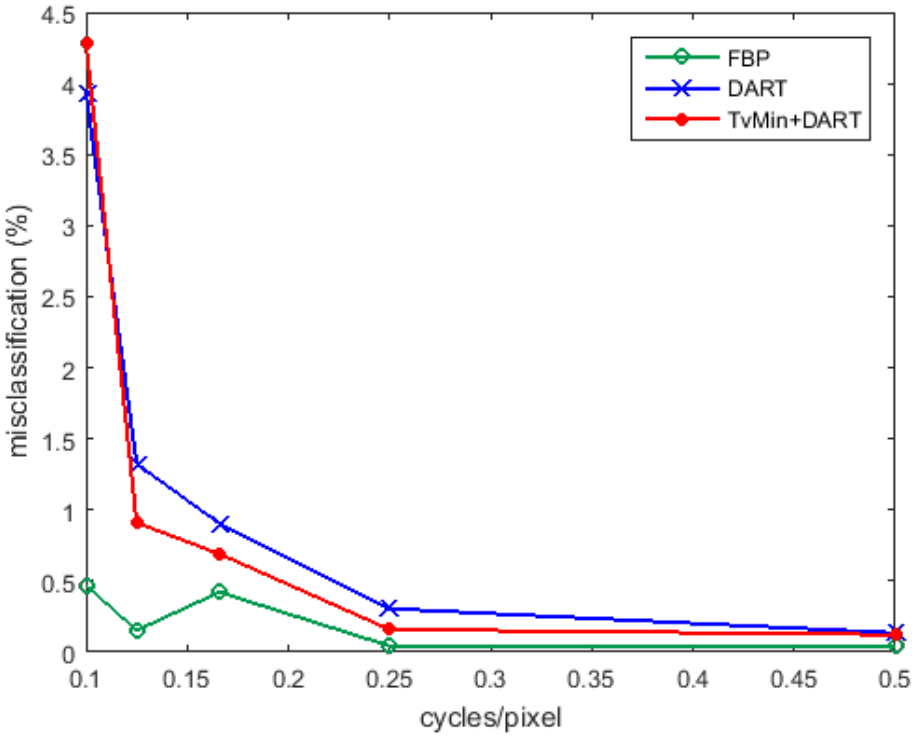

(a)

Figure 5.17: Misclassification with respect to cycles/pixel

5.5 Experiments on Converge Rate

In this section, the converge rate of the DART and the TvMin+DART algorithms are compared in terms of the misclassification and the root means squared projection error (RMSPE), by using Phantom-2, Phantom-3 and Phantom-5. While $k = 100$ iterations were used for Phantom-1, $k = 200$ iterations were performed for Phantom-3 and Phantom-5. All graphics show an almost monotonically decreasing behaviour. In Fig. 5.20, the misclassification remains around 24% and doesn't reach to the region of the exact solution, as it is predicted from the previous experiments. For Phantom-2, whose size is 256 by 256; the reconstruction time of the DART was 11.22 seconds, while 12.63 seconds were elapsed by the TvMin+DART. The reconstruction of Phantom-3, whose size is 512 by 512, took 107 seconds by the DART and 118 seconds by the proposed algorithm. Experiments were done on a single CPU core.

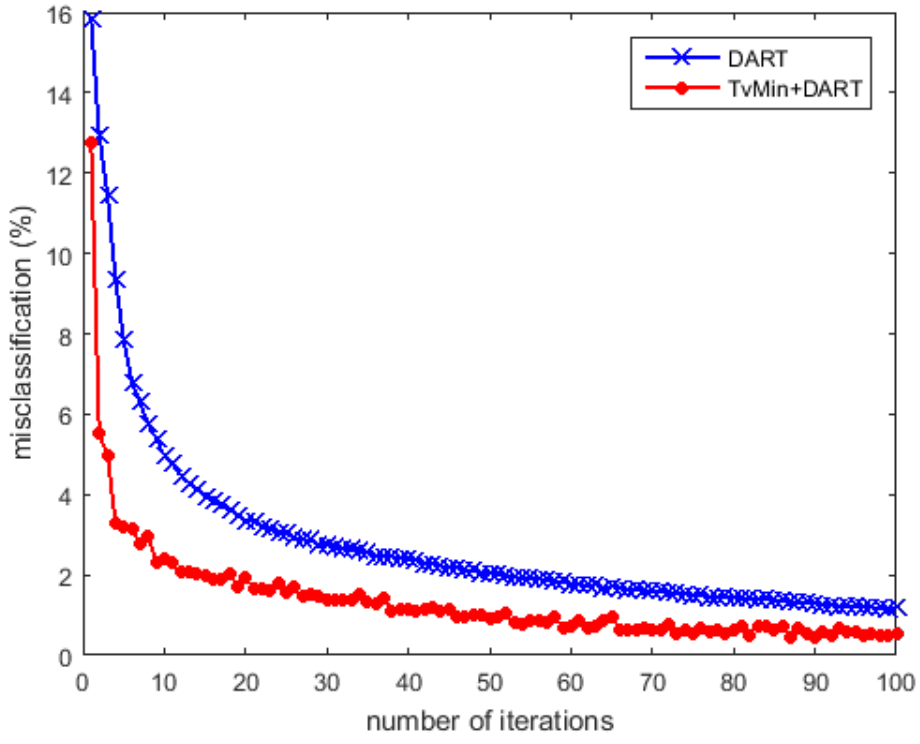

(a)

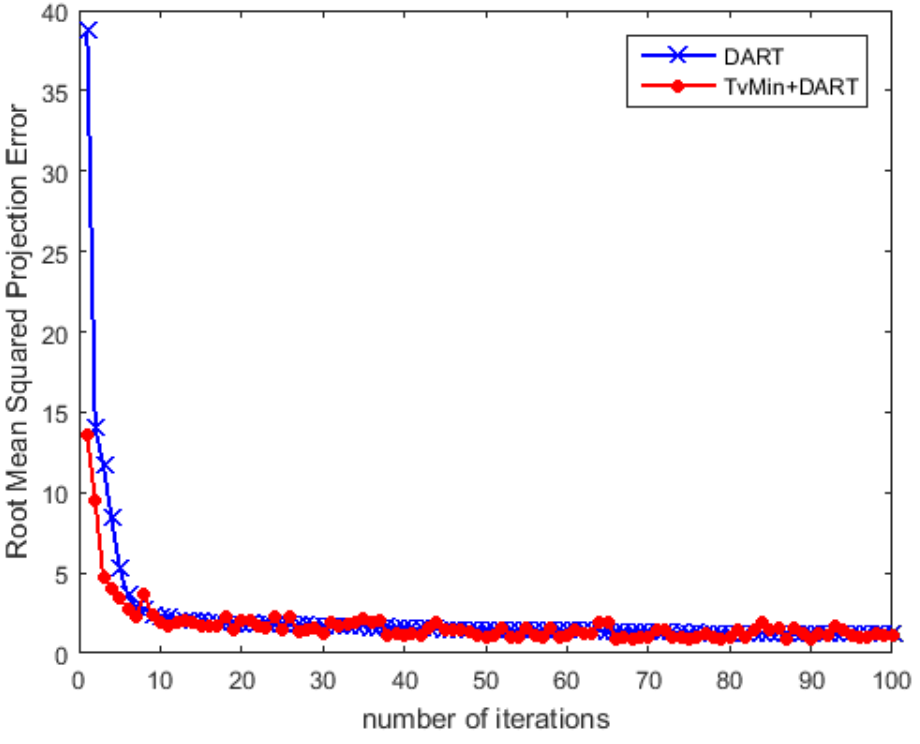

(b)

Figure 5.18: The converge rate for Phantom-2: (a) the misclassification and (b) the root mean squared projection error (RMSPE), with respect to the number of iterations, where $s = 6$

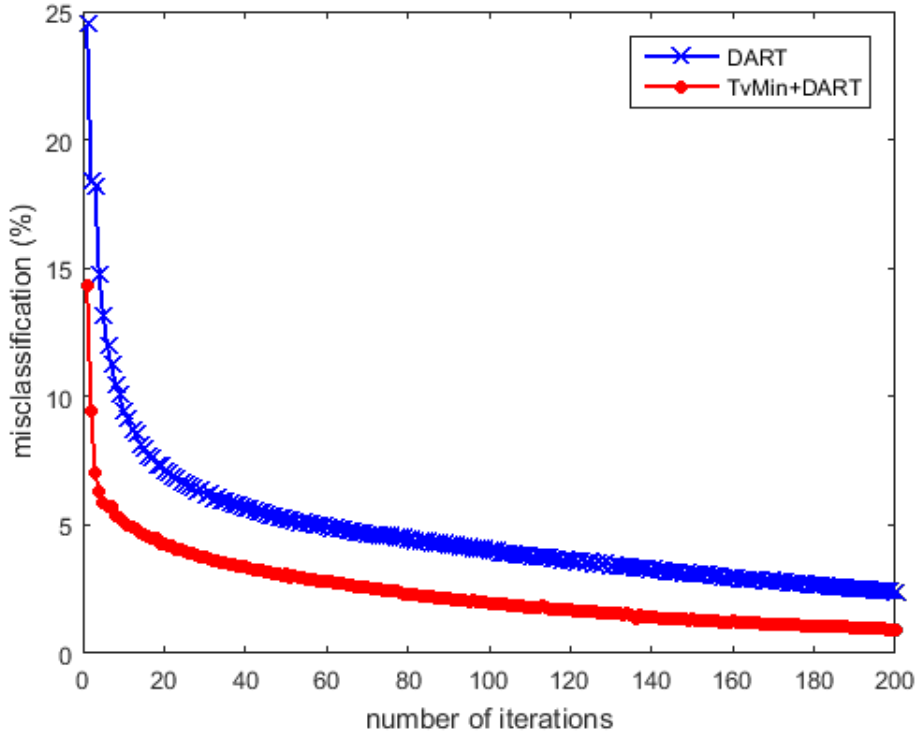

(a)

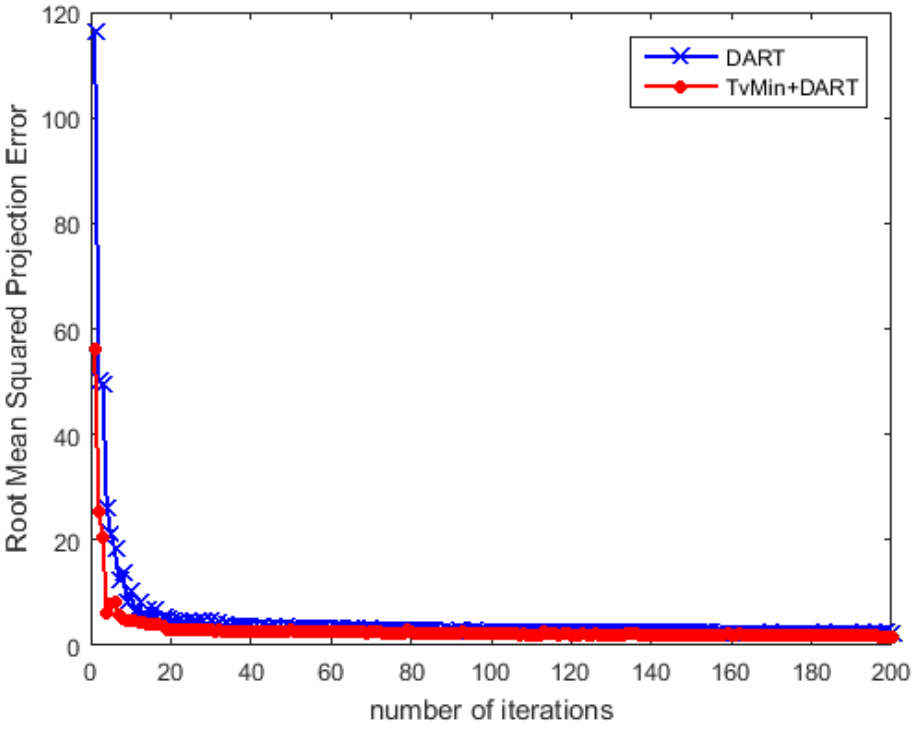

(b)

Figure 5.19: The converge rate for Phantom-3: (a) the misclassification and (b) the root mean squared projection error (RMSPE), with respect to the number of iterations, where $s = 14$

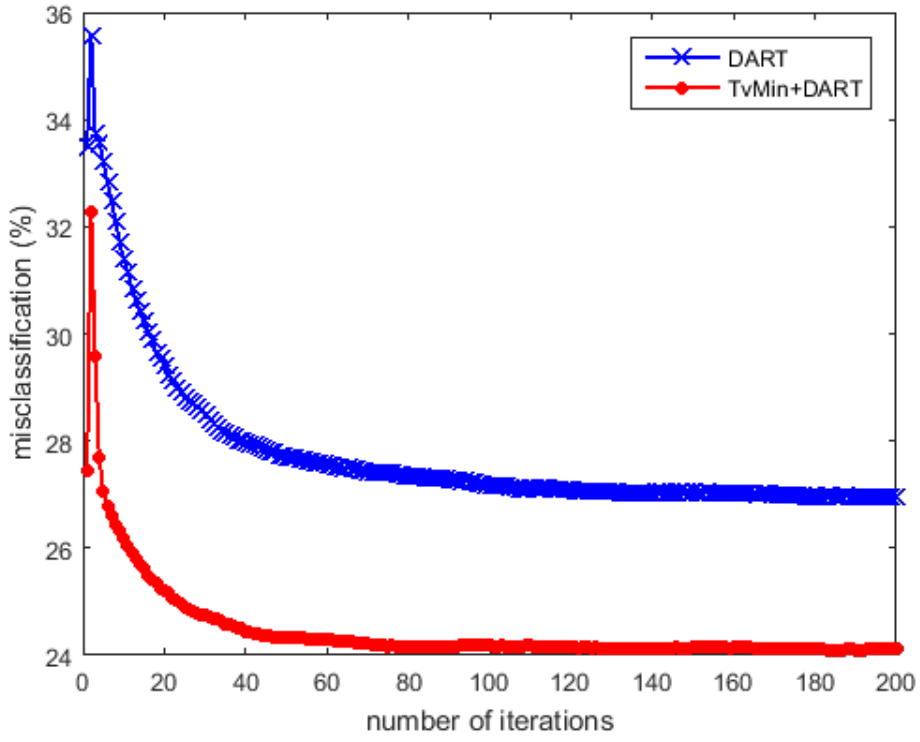

(a)

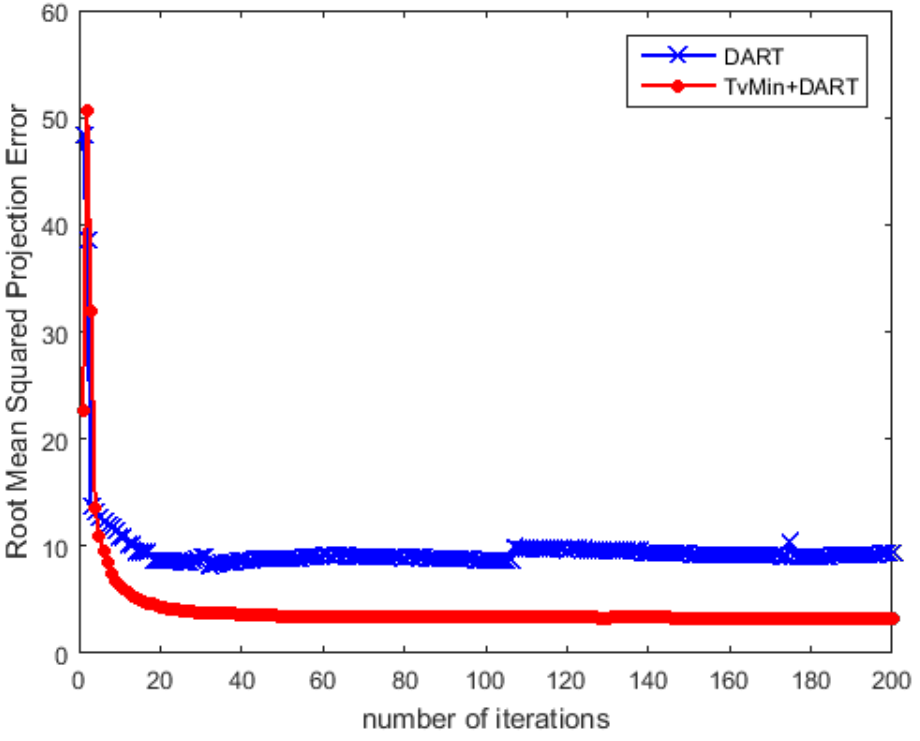

(b)

Figure 5.20: The converge rate for Phantom-5: (a) the misclassification and (b) the root mean squared projection error (RMSPE), with respect to the number of iterations, where $s = 60$

5.6 Gray Level Estimation

In this section, the results of the gray level estimation procedure are presented for the TvMin+DART algorithm. The experiments were started with the gray levels $\{0.3, 0.7\}$ for each phantom, although the exact gray levels were $\{0, 1\}$, and the final labels were estimated as stated in Fig. 5.21. In Fig. 5.22, Fig. 5.23 and Fig. 5.24, the converge behaviour of the algorithm is investigated for Phantom-2, Phantom-3 and Phantom-4, respectively. For this purpose, RMSE and RMSPE are used and as it can be seen in especially Fig. 5.24, high fluctuations are encountered for Phantom-4. Different number of projections are used for each phantom, s = 8, 10, 20 and 40 for Phantom 1 to 4, respectively.

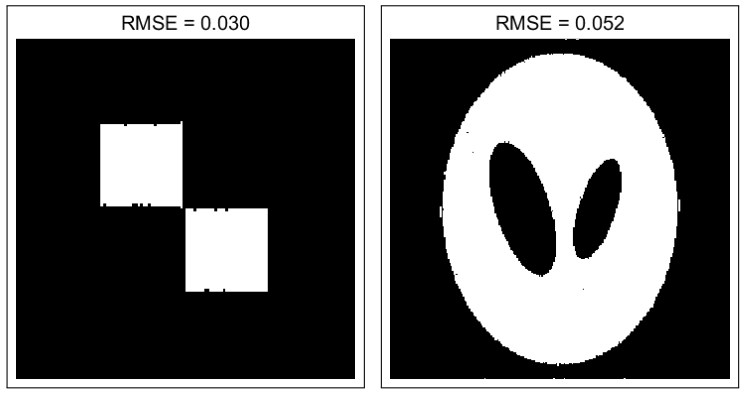

(a) Phantom-1, $s = 8$ (b) Phantom-2, $s = 10$

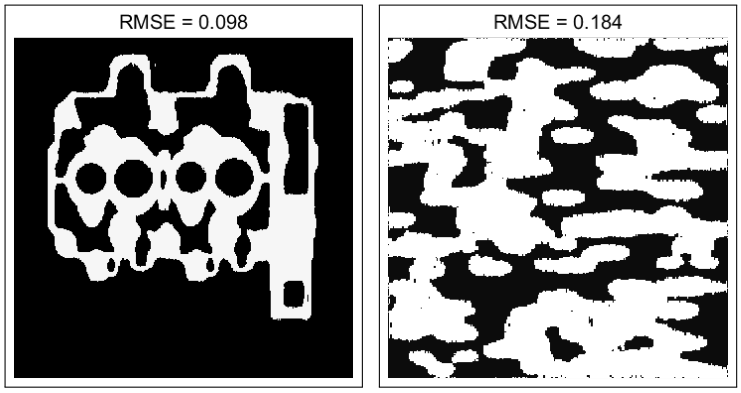

(c) Phantom-3, $s = 20$ (d) Phantom-4, $s = 40$

Figure 5.21: TvMin+DART with gray level estimation, started with the gray levels = $\{0.3, 0.7\}$ and reconstructed phantoms with labels (a) $\{0.001, 1.005\}$, (b) $\{0.001, 1.002\}$, (c) $\{0, 0.980\}$, (d) $\{0.009, 0.985\}$

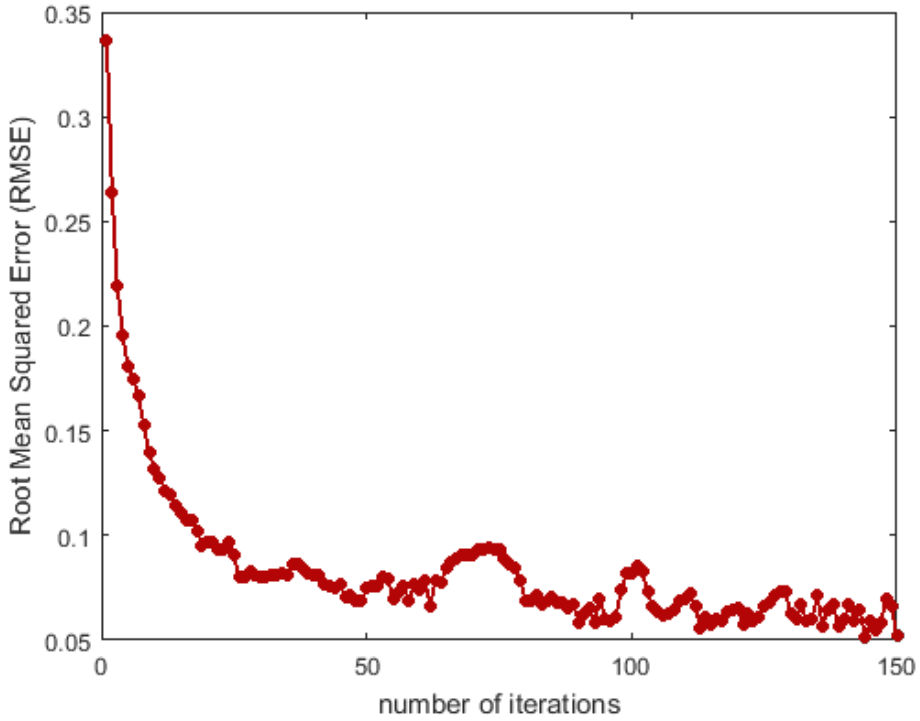

(a)

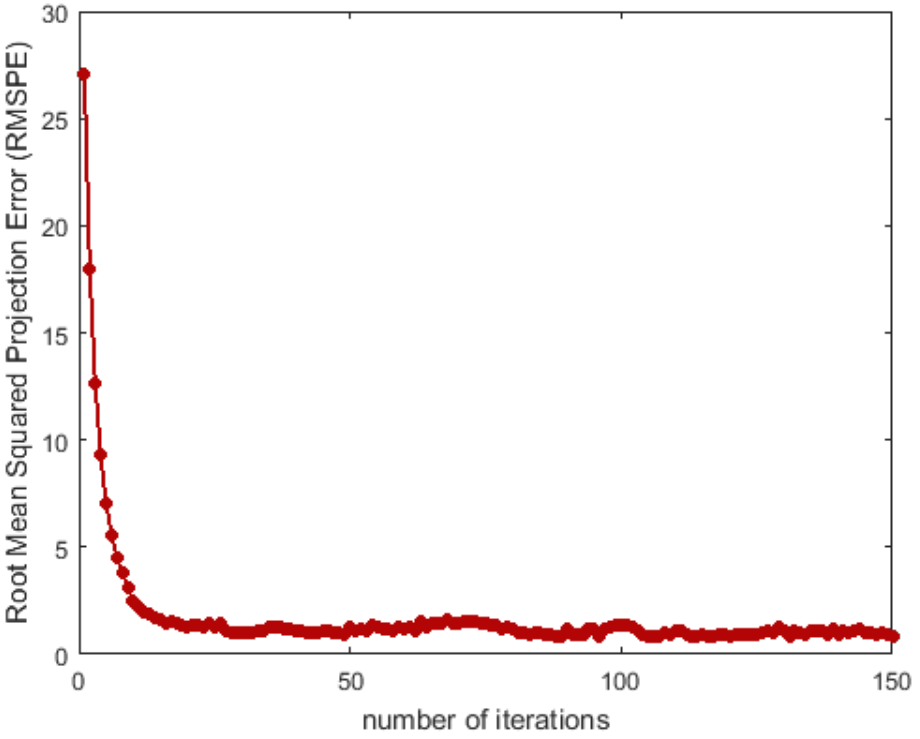

(b)

Figure 5.22: TvMin+DART with gray level estimation, converge rate for Phantom-2: (a) RMSE and (b) RMSPE, with respect to the number of iterations, where $s = 10$

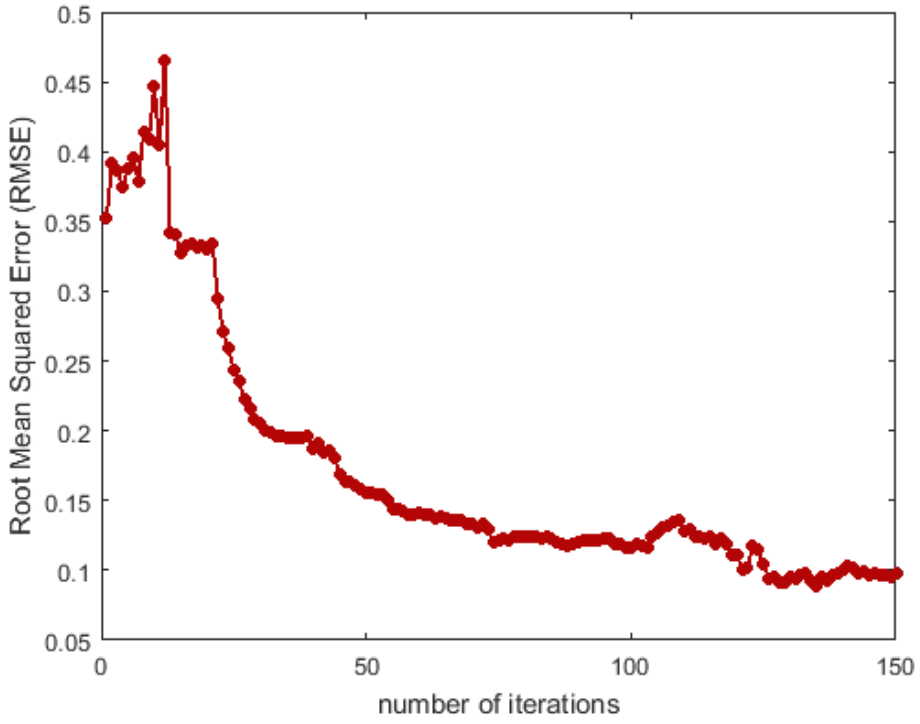

(a)

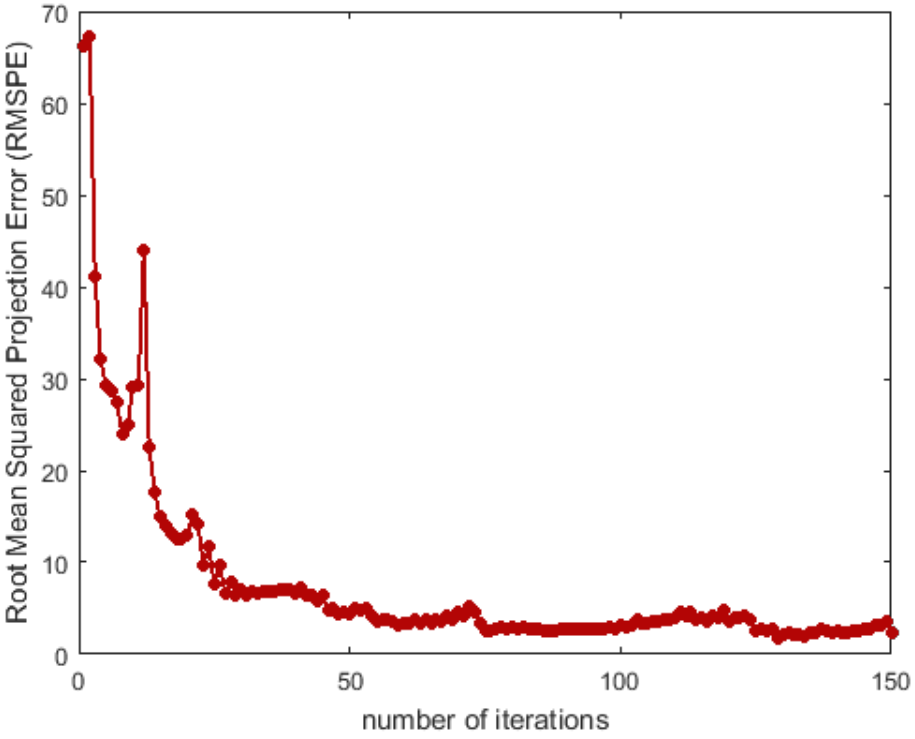

(b)

Figure 5.23: TvMin+DART with gray level estimation, converge rate for Phantom-3: (a) RMSE and (b) RMSPE, with respect to the number of iterations, where $s = 20$

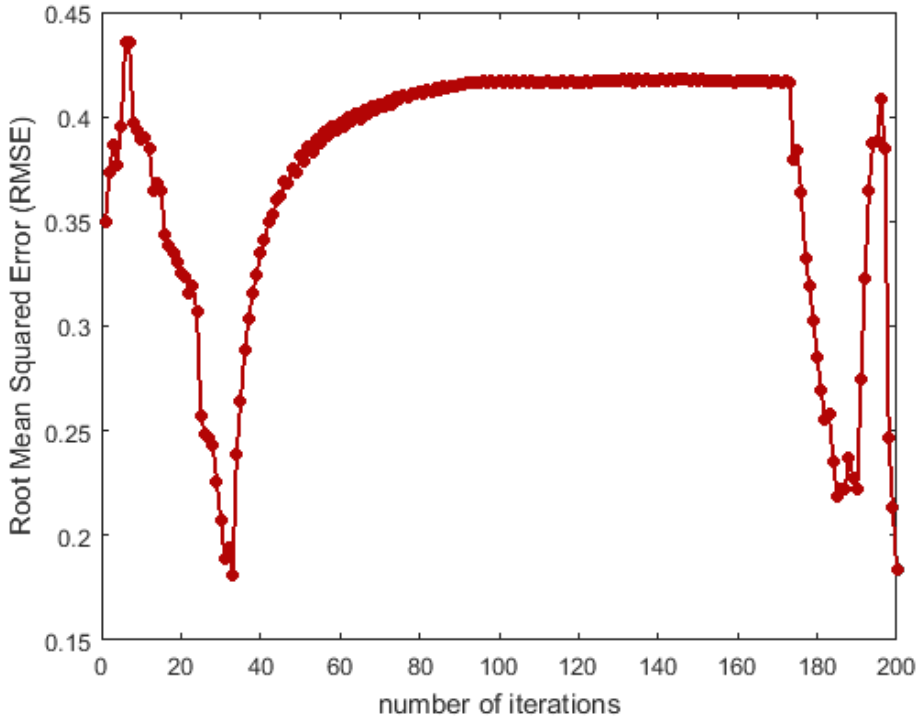

(a)

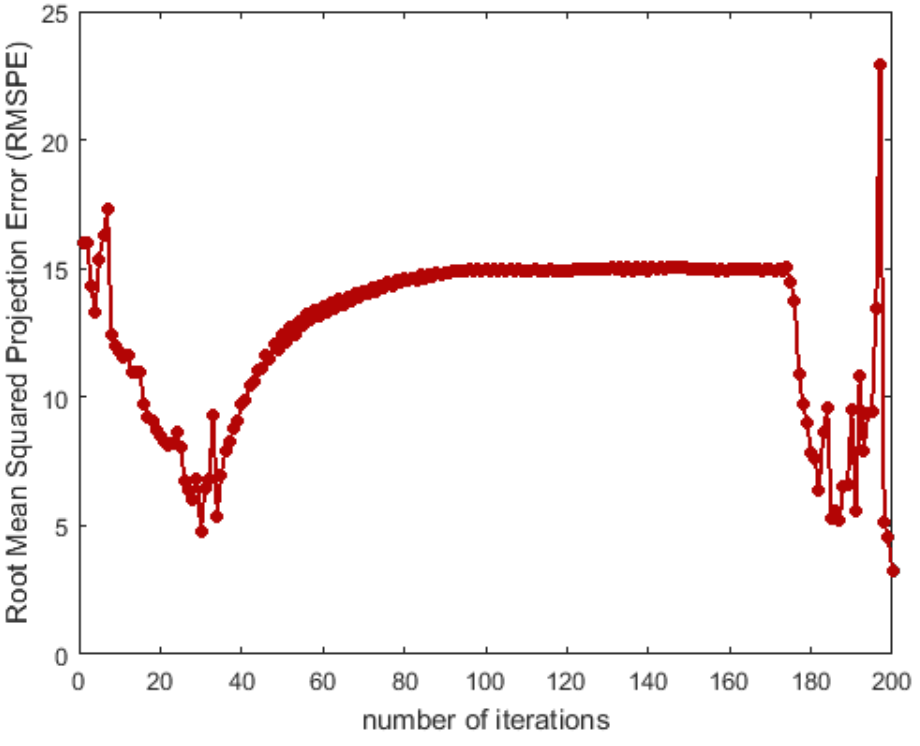

(b)

Figure 5.24: TvMin+DART with gray level estimation, converge rate for Phantom-4: (a) RMSE and (b) RMSPE, with respect to the number of iterations, where $s = 40$

6. CONCLUSIONS AND RECOMMENDATIONS

This study has been focussed on the problem of reconstruction from incomplete projections, investigated the DART algorithm, which was developed to accomplish this goal and proposed a multi-staged approach to improve the capabilities of the DART algorithm. The proposed approach considers three things about the original DART: (1) the algorithm that is used to compute the initial estimate, (2) selection of the threshold that is used to discretize the continuous reconstruction and (3) estimation of the gray levels in case they are not known in advance. For the first one, a total variation minimization technique (TvMin) is suggested, since it is famous with its ability of preserving high frequency regions and computing sharper, so easy-to-segment, reconstructions. This suggestion is supported by the simulation experiments that are presented in the previous chapter. Second, a threshold selection procedure, which is based on both the histogram and the projection data, is described in order to select a threshold that satisfies the available projection measurements and accomplish this in a computationally efficient manner. This procedure first counts the valleys of the histogram and estimates that many candidate thresholds, using a global thresholding method. Next, the optimum threshold is chosen among the candidates such that the projection error is minimized. Here, the cost function is also regularized with a total variation term. Third, a gray level estimation procedure is formulated such that the labels which minimizes the projection error are chosen in each iteration. The proposed algorithm is experimented in terms of accuracy, robustness and converge behaviour, by using various phantom samples. Its accuracy is compared to the original DART and the FBP algorithms, with respect to the several number of projections and several angular ranges, to simulate a reconstruction process with incomplete data. Moreover, the robustness of the proposed method is also compared to its two alternatives, with respect to noise in projection data. Gray level estimation experiments are carried out separately and the results are obtained in terms of the errors in the image and the projection domain as a function of the total number of iterations. Based on the studies, the following conclusions are drawn. The negative effects of limiting either the number

of projections (while keeping the range as full) or the angular range are gradual and in almost same fashion for all considered algorithms. However, the FBP algorithm is highly sensitive to noise when compared to the DART and the proposed method. It is also observed that the reconstruction quality highly depends on the morphology of the phantom. When the phantom is rigid, homogeneous, symmetrical and has a relatively low ratio of the edge pixels to the total number of pixels, the DART and the proposed method are producing more reasonable results, in comparison to the FBP, and these results show that the proposed method yields more accurate reconstructions than the DART algorithm in almost all experiments. On the other hand, its robustness to noise is comparable to the DART, just like its converge behaviour. With the gray level estimation experiments, it is observed that the proposed algorithm is able to compute reconstructions with the labels very close to the exact gray levels, however this situation is not guaranteed, especially for some phantoms, since it may show a non-stable behaviour when a local optimum is encountered.

This study and the simulation experiments call for new questions to be asked. Can the proposed method be developed such that the images, which have a high ratio of the edge pixels to the total number of pixels, can also be accurately and efficiently reconstructed? Can the projection geometry be used for this purpose, for instance, can the projections acquired from different angles and the reconstructions of them be exploited to obtain the update pixels, instead of focusing on the boundary regions? Also, it is observed that the proposed threshold selection procedure works better, when a smaller smoothing filter is used for the update pixels. However, all simulation experiments are done using a filter whose size is sufficient for both iterative algorithms. Can some more experiments, which are carried out with smaller filter but increased number iterations to estimate the initial guess, give more reasonable results on behalf of the proposed algorithm? Can the proposed threshold selection procedure be developed by using a penalty term? Furthermore, is it possible to enforce the results of each update, performed for each ray, to be equal to one of the gray levels from a predefined level set, meaning to change the conventional ART in a quantized fashion? All of these questions will be subject of the forthcoming studies by the author.

REFERENCES

[1] **Herman, G.T. and Kuba, A.** (2012). *Discrete tomography: Foundations, algorithms, and applications*, Springer Science & Business Media.

[2] **Cierniak, R.**, (2011). Some Words About the History of Computed Tomography, X-Ray Computed Tomography in Biomedical Engineering, Springer, pp.7–19.

[3] **Herman, G.T.** (2009). *Fundamentals of computerized tomography: image reconstruction from projections*, Springer Science & Business Media.

[4] **Kaczmarz, S.** (1937). Ängenäherte Auflösung von Systemen linearer Gleichungen, *Bull. Internat. Acad. Polon. Sci. Cl. A.*, ***35***, 355–357.

[5] **Batenburg, K.J. and Sijbers, J.** (2011). DART: A Practical Reconstruction Algorithm for Discrete Tomography., *IEEE Transactions on Image Processing*, ***20***(9), 2542–2553.

[6] **Gordon, R.**, **Bender, R. and Herman, G.T.** (1970). Algebraic reconstruction techniques (ART) for three-dimensional electron microscopy and x-ray photography, *Journal of Theoretical Biology*, ***29***, 471–481.

[7] **Gordon, R. and Herman, G.T.** (1971). Reconstruction of Pictures from Their Projections., *Commun. ACM*, ***14***(12), 759–768.

[8] **Herman, G.T. and Lent, A.** (1976). Iterative reconstruction algorithms, *Computers in Biology and Medicine*, ***6***(4), 273–294.

[9] **Herman, G.T. and Napastek, A.** (1977). Fast image reconstruction based on a Radon inversion formula appropriate for rapidly collected data, *SIAM J. Appl. Math.*, ***33***, 511–533.

[10] **Andersen, A.H. and Kak, A.C.** (1984). Simultaneous algebraic reconstruction technique (SART): A superior implementation of the ART algorithm, *Ultrasonic Imaging*, ***6***(1), 81 – 94.

[11] **Gale, D.** (1957). A theorem on flows in networks., *Pacific J. Math.*, ***7***(2), 1073–1082.

[12] **Batenburg, K.J.** (2008). A Network Flow Algorithm for Reconstructing Binary Images from Continuous X-rays., *Journal of Mathematical Imaging and Vision*, ***30***(3), 231–248.

[13] **Liao, H.Y. and Herman, G.T.** (2005). A Coordinate Ascent Approach to Tomographic Reconstruction of Label Images from a Few Projections, *Discrete Appl. Math.*, ***151***(1-3), 184–197.

[14] **Batenburg, K.J. and Sijbers, J.** (2007). DART: a fast heuristic algebraic reconstruction algorithm for discrete tomography, *Image Processing, 2007. ICIP 2007. IEEE International Conference on*, volume 4, IEEE, pp.IV–133.

[15] **Otsu, N.** (1979). A Threshold Selection Method from Gray-Level Histograms, *IEEE Transactions on Systems, Man and Cybernetics*, ***9***(1), 62–66.

[16] **Batenburg, K.J. and Sijbers, J.** (2009). Adaptive thresholding of tomograms by projection distance minimization, *Pattern Recognition*, ***42***(10), 2297–2305.

[17] **van Aarle, W.**, **Batenburg, K.J. and Sijbers, J.** (2012). Automatic parameter estimation for the discrete algebraic reconstruction technique (DART)., *IEEE Transactions on Image Processing*, ***21***(11), 4608–4621.

[18] **Donoho, D.** (2006). Compressed sensing, *IEEE Transactions on Information Theory*, ***52***(4), 1289 – 1306.

[19] **Candès, E. and Wakin, M.** (2008). An introduction to compressive sampling, *IEEE Signal Processing Magazine*, ***25***(2), 21–30.

[20] **Chang, T.C.**, **He, L. and Fang, T.** (2006). MR image reconstruction from sparse radial samples using Bregman iteration, *Proceedings of the 13th Annual Meeting of ISMRM, Seattle*, volume696.

[21] **Rudin, L.**, **Osher, S. and Fatemi, E.** (1992). Nonlinear total variation based noise removal algorithms, *Physica D.*, ***60***, 259–268.

[22] **Chambolle, A. and Lions, P.L.** (1997). Image recovery via total variation minimization and related problems, *Numer. Math.*, ***76***, 167–188.

[23] **Chambolle, A.** (2004). An algorithm for total variation minimization and applications, *Journal of Mathematical Imaging and Vision*, ***20***, 89–97.

[24] **Chambolle, A.**, **Caselles, V.**, **Novaga, M.**, **Cremers, D. and Pock, T.** (2009). An introduction to Total Variation for Image Analysis (lecture notes), *HAL archieves, hal-00437581*.

[25] **Lauzier, P.T.**, **Qi, Z.**, **Zambelli, J.**, **Bevins, N. and Chen, G.H.** (2012). Interior tomography in x-ray differential phase contrast CT imaging, *Physics in Medicine and Biology*, ***57***(9), N117.

[26] **Yang, J.**, **Yu, H.**, **Jiang, M. and Wang, G.** (2012). High-order total variation minimization for interior SPECT, *Inverse Problems*, ***28***(1), 015001.

[27] **Chen, G.H.**, **Tang, J. and Leng, S.** (2008). Prior image constrained compressed sensing (PICCS): a method to accurately reconstruct dynamic CT images from highly undersampled projection data sets, *Medical Physics*, ***35***(2), 660–663.

[28] **Herman, G.T. and Davidi, R.** (2008). Image reconstruction from a small number of projections, *Inverse Problems*, ***24***(4).

[29] **Kak, A.C. and Slaney, M.**, (1987). Principles of Computerized Tomographic Imaging, IEEE Press, New York, 2001 edition.

[30] **Gregor, J.M. and Benson, T.** (2008). Computational Analysis and Improvement of SIRT, *IEEE Trans. Med. Imaging*, ***27***(7), 918–924.

[31] **Tabak, F.** (2012). Robust Algorithms for Discrete Tomography, *Ph.D. thesis*, Delft University of Technology.

[32] **Donoho, D.L.** (2005). Neighborly polytopes and sparse solutions of underdetermined linear equations.

[33] **Li, C.** (2011). Compressive sensing for 3D data processing tasks: applications, models and algorithms, *Ph.D. thesis*, Rice University, Houston, TX, USA.

[34] **Candès, E.J. and Tao, T.**, (2006), Near Optimal Signal Recovery From Random Projections: Universal Encoding Strategies?

[35] **Goldfarb, D. and Yin, W.** (2004). Second-order cone programming methods for total variation-based image restoration, *SIAM Journal of Scientific Computing*, 622–645.

[36] **Li, C.** (2009). Compressive Sensing for 3D Data Processing Tasks: Applications, Models and Algorithms, *Ph.D. thesis*, Rice University, Houston, Texas.

[37] **Huang, D.Y.**, **Lin, T.W. and Hu, W.C.** (2011). Automatic multilevel thresholding based on two-stage Otsu's method with cluster determination by valley estimation, *International Journal of Innovative Computing, Information and Control*, ***7***(10), 5631–5644.

[38] **Huang, D.Y. and Wang, C.H.** (2009). Optimal Multi-level Thresholding Using a Two-stage Otsu Optimization Approach, *Pattern Recogn. Lett.*, ***30***(3), 275–284.

[39] **Hansen, P.C. and Saxild-Hansen, M.** (2012). AIR Tools - A MATLAB Package of Algebraic Iterative Reconstruction Methods, *J. Comput. Appl. Math.*, ***236***(8), 2167–2178.

[40] **Candes, E. and Romberg, J.**, (2005), L1-magic: Recovery of Sparse Signals via Convex Programming.

[41] **Esedoglu, S.**, **Chan, T.**, **Park, F. and Yip, A.** (2005). Recent developments in total variation image restoration, *Mathematical Models of Computer Vision*, ***17***.

[42] **Zeng, G.L.** (2010). *Medical Image Reconstruction: a conceptual tutorial*, Springer Berlin Heidelberg, Berlin, Heidelberg.

[43] **Zhu, Z.**, **Wahid, K.A.**, **Babyn, P.**, **Cooper, D.**, **Pratt, I. and Carter, Y.** (2013). Improved Compressed Sensing-Based Algorithm for Sparse-View CT Image Reconstruction., *Comp. Math. Methods in Medicine*, ***2013***.

CURRICULUM VITAE

Name Surname: Ezgi Demircan-Türeyen

Place and Date of Birth: Turkey, 1987

Adress: Istanbul/Turkey

B.Sc.: Istanbul Kultur University Department of Computer Engineering, Istanbul, Turkey (2010)

M.Sc.: Istanbul Technical University, Department of Computer Engineering, Istanbul, Turkey (2015)

PUBLICATIONS/PRESENTATIONS ON THE THESIS

- **Demircan-Tureyen E.**, Kamasak M.E., 2015: A Compressed Sensing Based Approach on Discrete Algebraic Reconstruction Technique. *37th Annual International Conference of The IEEE Engineering in Medicine and Biology Society EMBC'15*, August 25-29 2015, Milano, Italy. (accepted)